HHS Public Access

Author manuscript

Nat Struct Mol Biol. Author manuscript; available in PMC 2020 April 14.

Published in final edited form as:

Nat Struct Mol Biol. 2019 November ; 26(11): 999–1012. doi:10.1038/s41594-019-0313-z.

PRMT5 methylome profiling uncovers a direct link to splicing regulation in acute myeloid leukemia

Aliaksandra Radzisheuskaya[1,2,3], **Pavel V Shliaha**[4,5], **Vasily Grinev**[6], **Eugenia Lorenzini**[1,2], **Sergey Kovalchuk**[4,7], **Daria Shlyueva**[1,2], **Vladimir Gorshkov**[4], **Ronald C Hendrickson**[5], **Ole N Jensen**[4], **Kristian Helin**[1,2,3]

[1]Biotech Research and Innovation Centre (BRIC), Faculty of Health and Medical Sciences, University of Copenhagen, Copenhagen, Denmark.

[2]The Danish Stem Cell Center (Danstem), University of Copenhagen, Faculty of Health and Medical Sciences, University of Copenhagen, Copenhagen, Denmark.

[3]Cell Biology Program and Center for Epigenetics, Memorial Sloan Kettering Cancer Center, New York, New York, USA.

[4]Department of Biochemistry and Molecular Biology, VILLUM Center for Bioanalytical Sciences, University of Southern Denmark, Odense, Denmark.

[5]Microchemistry and Proteomics Core Facility, Memorial Sloan Kettering Cancer Center, New York, New York, USA.

[6]Department of Genetics, Faculty of Biology, Belarusian State University, Minsk, Belarus.

[7]Laboratory of bioinformatic methods for combinatorial chemistry and biology, Shemyakin-Ovchinnikov Institute of Bioorganic Chemistry, Moscow, Russia.

Abstract

Protein arginine methyltransferase 5 (PRMT5) has emerged as a promising cancer drug target, and three PRMT5 inhibitors are currently in clinical trials for multiple malignancies. In this study, we investigated the role of PRMT5 in human acute myeloid leukemia (AML). Using an enzymatic dead version of PRMT5 and a PRMT5-specific inhibitor, we demonstrated the requirement of the catalytic activity of PRMT5 for the survival of AML cells. We then identified PRMT5 substrates using multiplexed quantitative proteomics and investigated their role in the survival of AML cells. We found that the function of the splicing regulator SRSF1 relies on its methylation by PRMT5 and that loss of PRMT5 leads to changes in alternative splicing of multiple essential genes. This explains the requirement of PRMT5 for leukemia cell survival. We show that PRMT5 regulates

Correspondence: Kristian Helin, helink@mskcc.org.

Author contributions

Conceptualization, A.R. and K.H.; Methodology, A.R., P.V.S., and V.Gr.; Investigation, A.R., P.V.S., V.Gr., E.L., S.K., D.S., V.Go.; Writing – Original Draft, A.R. and K.H.; Writing – Review & Editing, all authors; Visualization, A.R., P.V.S., V.Gr.; Funding Acquisition, A.R., P.V.S, O.N.J, and K.H..; Supervision, R.C.H., O.N.J and K.H.

Competing interests

The authors declare no competing interests

binding of SRSF1 to mRNAs and proteins and provide potential biomarkers for the treatment response to PRMT5 inhibitors.

Introduction

Arginine methylation is an ubiquitous protein posttranslational modification in mammals[1], catalyzed by the PRMT protein family that transfers a methyl group from S-adenosylmethionine (SAM) to the guanidine nitrogen atom of arginine. There are three forms of methylated arginines in mammals: ω-N^G-monomethylarginine (MMA), asymmetric ω-N^G,N^G-dimethylarginine (ADMA), and symmetric ω-N^G,N'^G-dimethylarginine (SDMA), and the PRMT enzymes are classified depending on the type of modification they generate[2]. Functionally, protein arginine methylation is known to affect binding interactions. The bulky methyl groups can prevent access to the potential hydrogen bond donors in arginine groups, and, thereby, inhibit protein interactions. At the same time, arginine methylation is known to facilitate the interaction with Tudor domains on proteins[3].

Protein methyltransferase 5 (PRMT5) has recently emerged as a promising cancer drug target, and three PRMT5 inhibitors are currently in clinical trials for a range of solid and blood cancers[4,5]. PRMT5 was shown to act as an oncoprotein in multiple malignancies, conferring aggressiveness and promoting cell proliferation[6,7]. Moreover, several recent reports have demonstrated a selective sensitivity of cancers with 9p21 deletion to the knockdown of *PRMT5*, due to synthetic lethality with the deleted *MTAP* (methylthioadenosine phosphorylase) gene[8–10]. Since 9p21 is a very frequent deletion present in about 14% of all cancers[11], PRMT5 inhibition represents an exciting therapeutic strategy for cancers with, in particular, this chromosomal aberration.

PRMT5 belongs to the class II arginine methyltransferases, as it catalyzes monomethylation and symmetrical dimethylation of arginines on proteins[12,13]. It acts in a complex with WDR77 (also known as MEP50 and WD45)[14], responsible for proper orientation of the PRMT5 substrates[15,16]. Several nuclear and cytoplasmic substrates of PRMT5 have been reported, which are involved in different cellular processes, including transcription, DNA damage response, splicing, translation and cell signaling[6,7]. However, further studies are required to understand the mechanism by which PRMT5 contributes to tumorigenesis and normal cellular physiology. In this study, we aimed at identifying substrates regulated by PRMT5, which are essential for cancer cell proliferation.

Results

The catalytic activity of PRMT5 is required for proliferation of MLL-AF9-rearranged AML cells

To assess the requirement for *PRMT5* expression in AML cells, we used CRISPR interference (CRISPRi) and CRISPR knockout (CRISPRko) (Extended Data Fig.1a). For CRISPRi, the cells were transduced with a lentivirus constitutively expressing the catalytically dead Cas9 (cdCas9) protein fused to a KRAB repression domain[17,18]. Upon the transduction of the THP-1-cdCas9-KRAB cells with two independent sgRNAs

complementary to the *PRMT5* transcription start site, efficient *PRMT5* gene repression was observed (Extended Data Fig.1b, c). This led to decreased levels of global symmetrical arginine dimethylation (Extended Data Fig.1d) as well as substantial cell proliferation defects (Extended Data Fig.1e). A similar effect was observed using MOLM-13-cdCas9-KRAB (Extended Data Fig.1f, g). Using a similar setup, we also confirmed the requirement of the PRMT5 co-factor WDR77 for the growth of AML cells (Extended Data Fig.1h, i). The requirement for PRMT5 for cell proliferation was also validated in human THP-1, MOLM-13, MONOMAC-6 and mouse MLL-AF9-wtCas9 leukemia cells using the CRISPRko system (Extended Data Fig.1j). Taken together, these data demonstrate that PRMT5 depletion leads to growth inhibition of AML cells.

To investigate whether the enzymatic activity of PRMT5 is important for its function in human AML, we established THP-1-cdCas9-KRAB cell lines stably overexpressing either wild type (wt) or catalytically dead (cd) versions of PRMT5. Next, we transduced them with lentiviruses expressing sgRNAs that bind the *PRMT5* promoter and together with the cdCas9-KRAB induce the knockdown (KD) of the endogenous *PRMT5* locus. While the exogenously expressed wtPRMT5 cDNA induced complete rescue of global symmetrical arginine dimethylation levels and cell growth (Fig.1a, b, c), cdPRMT5 conferred a dominant negative phenotype (Fig. 1d–f). Particularly, its expression led to further decrease in arginine methylation, when the Stuffer cells demonstrate only a slight decrease (Fig.1e). Moreover, the effect of knocking down endogenous *PRMT5* on cell proliferation was stronger in the cells expressing cdPRMT5 (Fig.1f). Consistently, we found that treatment of THP-1 cells with the specific PRMT5 inhibitor (EPZ015666) decreases global levels of symmetrical arginine dimethylation (Extended Data Fig.2a) and negatively impacts cell proliferation (Fig. 1g), further confirming the requirement of the enzymatic activity of PRMT5 for cell growth. Finally, exogenous *PRMT5* overexpression increased cell resistance to inhibitor treatment, demonstrating the specificity of PRMT5 inhibition (Extended Data Fig.2b, c).

Identification of novel PRMT5 substrates in human AML cells

Given the essential nature of the enzymatic activity of PRMT5, we performed systematic identification of its substrates by LC-MS/MS-based proteomics with the use of isobaric mass tag labelling approach for quantitation[19], as outlined in Fig.2a. Ten samples were co-analyzed in the TMT10plex experiment: four biological replicates of cells transduced with a non-targeting sgRNA and three biological replicates of cells transduced with two independent sgRNAs inducing *PRMT5* knockdown. Deep and reliable profiling of proteins and methylated peptides was achieved by two strategies. First, we performed three two-dimensional LC separations with a different number of first dimension (high pH RP) fractions and different lengths of the second dimension (low pH RP) gradient. Secondly, we enriched for peptides with monomethylated and symmetrically dimethylated arginines using immunoaffinity purification.

To ensure high accuracy of quantitation we analyzed the samples on an Orbitrap Fusion LUMOS platform using multinotch SPS[20], and removed peptide spectrum matches (PSMs) prone to inaccurate quantitation (with low intensity of reporter ions or high degree of contamination with co-selected peptides). Proteins were included, if their quantitation was

based on at least two proteotypic peptides. After application of the filtering criteria we identified 384765 PSMs and 125801 peptides from 7426 proteins (Supplementary Table 1). 2962 proteins were differentially expressed in both *PRMT5* sgRNA samples. For all 2962 proteins, the change in abundance between the two *PRMT5* sgRNA conditions and the control sample was in the same direction (Fig.2b). Furthermore, PRMT5 and its co-factor WDR77 were the two most downregulated proteins (Fig.2c). *PRMT5* sgRNA-2 induced a better *PRMT5* knockdown (Fig.2c, Extended Data Fig.1b, c) and, consistently, higher absolute changes of 83% of regulated proteins, supporting that the observed protein changes are specific. Downregulated proteins were significantly enriched in components of DNA replication and repair pathways, while upregulated proteins were enriched in leukocyte granulation, RNA processing and vesicle transport categories (Fig.2d).

Combining the two approaches of deep 2D LC-MS and immunoenrichment (Fig.2a), we identified 1209 peptides with arginine methylation (Fig.2e). Relative abundances of modified peptides were divided by their corresponding protein abundances (Fig.2f, Supplementary Table 1), to ensure that the reported changes reflect site occupancy and not just changes in protein expression. 420 peptides from 183 different proteins were differentially methylated (q-value $\leq$0.1 in both PRMT5 sgRNA conditions). All the observed changes had the same direction in both PRMT5 sgRNA conditions (Fig.2g). To define a list of potential PRMT5 substrates, we selected proteins with at least one arginine monomethylation or dimethylation site decreased. This resulted in a set of 61 protein, which were enriched in proteins involved in RNA end processing, splicing and binding (Fig.2h, Supplementary Table 1).

To investigate which of the identified potential targets of PRMT5 could explain its requirement for the leukemic cell growth, we cross-referenced the list of the 61 arginine methylated protein with a previously published genome-wide CRIPSRko screen in human AML cell lines[21]. We selected 17 proteins that were shown to be required for AML cell growth (Extended Data Fig.3a), with the hypothesis that arginine methylation of these would be essential for their function. Next, for these 17 proteins we identified those directly targeted by PRMT5. We synthesized 25 amino acids parts of the protein sequences containing the identified differentially regulated arginine methylation sites and incubated these peptides with a recombinant PRMT5-WDR77 complex followed by mass spectrometry analysis. Peptides from 12 out of the 17 proteins demonstrated characteristic methylation mass shifts (single or multiple of +14 Da) and, hence, confirmed their proteins as PRMT5 substrates (Fig.3a, Extended Data Fig.3b). Most of the substrates contained several arginine methylation sites (e.g. SNRPB, SFPQ, SRSF1, PNN, CPSF6, CCT7, ALYREF, RPS10). In addition, we observed a tendency for more arginines in the vicinity of the methylated site, but none directly next to each other, resulting in a potential GRGRGR pattern as a PRMT5 consensus motif (Fig.3b).

Next, we confirmed that 11 out of the 12 identified protein substrates indeed are required for the proliferation of human AML cells (Fig.3c, d and Extended Data Fig.3c). Interestingly, the majority of these substrates are involved in different aspects of RNA metabolism and, particularly, mRNA splicing (Table 1, Fig.3e).

In summary, by combination of proteomics, in vitro methyltransferase assays and genetic studies we have identified 11 proteins as PRMT5 substrates that are also essential for the proliferation of AML cells. These proteins are highly enriched for regulators of RNA metabolism.

PRMT5 depletion leads to changes in alternative splicing in human AML cells

Several recent studies reported changes in alternative splicing as a result of *PRMT5* downregulation in glioma, lymphoma, fetal liver cells and several solid cancer cell lines[22–26]. However, mechanistic insights into which PRMT5 substrates regulate this process are lacking. Since the majority of the essential PRMT5 substrates we identified were previously implicated in RNA binding, processing (including splicing) and transport, we decided to profile differences in alternative splicing between the wild type and *PRMT5* KD AML cells. As before, THP-1-cdCas9-KRAB cells were transduced with a non-targeting sgRNA or an sgRNA against *PRMT5*, and the cells were subjected to RNA sequencing.

First, using the DESeq2[27] and edgeR-limma[28,29] approaches, we identified 2974 retained introns (RIs) in the transcriptome of THP-1 cells (Extended Data Fig. 4a, Supplementary Table 2). The retention of these introns was confirmed by Cufflinks[30] assembly of full-length transcripts (Extended Data Fig. 4b, c) and, for selected events, by qRT-PCR (see below). Next, we extended the list of the identified RIs with exons expressed in THP-1 cells, and applied DEXSeq[31] and limma-diffSplice[29] algorithms to detect the differentially used RIs (diffRIs) and exons following the *PRMT5* knockdown. We found that wild type and *PRMT5* KD cells differ in the usage of 415 RIs (Fig. 4a) and 1079 exons (data not shown) distributed over 321 and 777 individual genes, respectively. The vast majority of the diffRIs exhibit higher levels in the KD cells, indicating the tendency of the PRMT5-depleted cells to retain introns in mature RNA molecules (Fig. 4b), which is consistent with a previous report in glioma cells[22].

Next, using the limma-diffSplice[29] and JunctionSeq[32] approaches, we analyzed differential usage of the exon-exon junctions (EEJs) in the transcriptome of THP-1 cells upon the *PRMT5* knockdown. We found 719 differential EEJs (diffEEJs, Fig. 4c, Extended Data Fig. 4d, Supplementary Table 2) distributed over 572 individual genes. Among the identified diffEEJs, the majority are annotated by Ensembl, while about 13% of the upregulated and 4% of the downregulated EEJs represent novel EEJs (Fig. 4d). This suggests that rather than inducing aberrant splicing events, PRMT5 loss leads to the differential usage of already known isoforms. If we classify all the identified EEJs according to splicing modes, *PRMT5* KD mostly causes single or multiple exon skipping and alternative 5' and or 3' splice sites selection (Fig. 4e). Interestingly, we observed very small overlap between the differentially spliced and differentially expressed genes (Fig. 4f), suggesting that the detected alternative splicing differences rarely affect total mRNA expression levels.

To understand if there is a link between the differential splicing and the changes in arginine methylation of the splicing regulators identified as PRMT5 substrates, we focused on two factors that are known to bind RNA during the splicing process (SRSF1[33] and SFPQ[34,35]). We compared the frequency of their binding motifs in 100 nucleotides around the diffEEJs and non-diffEEJs, as well as around the diffRIs and non-diffRIs. Strikingly, the SRSF1

binding motif frequency was significantly higher both at the 5' and 3' splice sites of the diffEEJs (Fig. 4g, Extended Data Fig.4e), but not around the diffRIs (data not shown). The absolute number of SRSF1 motifs per splice site was significantly increased for the differential splicing events of both classes (Fig. 4h,i). Notably, the motifs of two SRSF1 interacting partners, SRSF2 and SRSF3, but not SRSF7, were also significantly enriched at the splice sites of the diffEEJs (Extended Data Fig. 4f, g and data not shown). At the same time, minimal differences in the frequency of the SFPQ motif were observed between the differential and non-differential splicing events (Fig. 4j, Extended Data Fig.4h).

To analyze whether changes in alternative splicing induced by the loss of PRMT5 bear similarities in different cells types, we compared the differential splicing events found in AML cells with the ones from a recently published study in U-87 MG glioma cells[22]. Interestingly, we observed many common differential splicing events using both retained intron and exon-exon junction analysis (Fig.4k, l, Supplementary Table 2). Moreover, we found that the SRSF1 motif is also significantly enriched in the differential EEJs in U-87 MG cells (Extended Data Fig.4i–l). Taken together, these findings suggest a potential common mechanism of alternative splicing regulation by PRMT5 via SRSF1 methylation.

In summary, our results show that loss of PRMT5 leads to numerous changes in alternative splicing events in human AML cells, particularly, increased exon skipping and higher frequency of retained introns. Motif analysis demonstrates a strong enrichment for the motif of the PRMT5 substrate SRSF1 among the differential exon-exon junctions.

PRMT5 loss induces alternative splicing and reduction in protein level of multiple essential genes

Since only a small proportion of the differentially spliced genes demonstrated a change in total mRNA levels, we hypothesized that alternative splicing can affect the protein level of a gene by changing mRNA translation efficiency or protein integrity or stability. Thus, we used the global proteomics data (Fig.2a) to analyze protein level changes of splicing-affected genes after *PRMT5* KD. Among the 825 genes with differential alternative splicing events (both differential EEJ and retained introns), 687 had reliably quantified protein levels and 88 of those demonstrated significant changes in protein expression, with the majority, 74, being downregulated upon the *PRMT5* KD (Fig.5a). To understand whether differential splicing of some of these genes could be linked to reduced proliferation in KD cells, we selected seven genes with affected splicing: *POLD1*, *POLD2*, *PPP1R7*, *PNISR*, *FDPS*, *PNKP* and *PDCD2*, which are essential according to published CRISPRko screens[36]. Using a CRISPRko competition assay, we independently confirmed their essentiality in human AML cells (Fig. 5b). The downregulation on protein level ranged from 25 to 50% (Fig.5c), but since the TMT-based proteomics experiments might be subject to ratio suppression, the differences could be more pronounced. Using the qRT-PCR, we validated all the identified differential splicing events in these genes (Fig.5d,e), and the results strongly correlated with the RNA-sequencing values (Fig.5f). In these selected events, we also observed an increased frequency of SRSF1 binding motifs around the differential splicing sites (Extended Data Fig. 5a, b).

To illustrate the potential functional consequences of the identified differential splicing events in the selected essential genes, we present two examples (Fig.5g, h). For *PDCD2*, differential splicing leads to early alternative transcription termination and, thereby, potential loss of a C-terminal domain (Fig.5g). For *PNKP*, a differentially retained intron between exons 5 and 6 of the gene contains a premature translation termination codon, which likely leads to nonsense-mediate mRNA decay (NMD) and or protein truncation (Fig.5h). To test whether alternative splicing of *PNKP* leads to NMD of its mRNA, we treated the cells, transduced with either a negative control or a *PRMT5* sgRNA, with emetine, a drug inhibiting NMD. This led to stabilization of the *PNKP* mRNA containing the retained intron with a more pronounced effect in the case of *PRMT5* KD (Fig.5i). This confirms that differential alternative splicing of *PNKP,* induced by the *PRMT5* knockdown, leads to the NMD of its mRNA.

In summary, PRMT5 depletion leads to changes in alternative splicing and protein downregulation of several essential genes in human AML cells. This likely contributes to the requirement of PRMT5 for cell survival.

Arginine methylation of SRSF1 is functionally important for cell survival

Next, we tested if PRMT5-mediated arginine methylation of an identified substrate regulates its function. To do this, we generated arginine-to-lysine mutants (R-to-K) of the identified PRMT5-mediated methylation sites in the essential substrates and assessed their functionality by performing rescue experiments of the corresponding gene knockdown or knockout. For this, we first established stable cell lines overexpressing either the wild type or mutant versions of the substrates and then delivered the sgRNAs to deplete the corresponding endogenous gene. As shown in Figure 6a, the R-K mutant proteins of nine substrates (SNRPB, SFPQ, CCT4, SUPT5H, PNN, CPSF6, ALYREF, CCT7 and RPS10), demonstrated comparable performance to the wild type version of the gene, suggesting that arginine methylation on those sites is not essential for their function and therefore cell survival (Fig.6a).

Overexpression of SRSF1 on top of the endogenous levels caused cell death in four different human AML cell lines, demonstrating tight regulation of its levels. Thus, we could not use the same strategy for the rescue experiments as above. To address this challenge, we transduced the THP-1-cdCas9-KRAB-2A-mCherry cells with an *SRSF1* wild type or triple R-to-K mutant cDNA simultaneously with the *SRSF1* knockdown sgRNA construct, also driving the BFP expression. This approach provides an opportunity for some knockdown cells to establish wild type SRSF1 levels and survive. 14 days after transduction we sorted out the BFP and mCherry double positive (dCas9 and sgRNA-positive) cells from each condition and assessed the source of their *SRSF1* expression by qRT-PCR. As expected, cells transduced with the wild type *SRSF1* transgene exhibited knockdown of the endogenous *SRSF1* and relied on the exogenous SRSF1 expression for their growth, indicating complete rescue (Fig.6b). At the same time, the surviving mutant- and Stuffer-transduced BFP and mCherry double positive cells demonstrated no efficient knockdown of the endogenous *SRSF1* (Fig.6b), demonstrating that for these samples we could only recover the cells that escaped the effect of *SRSF1* CRISPR interference. This shows that mutant

SRSF1 cannot substitute for the wild type and confirms that arginine methylation of SRSF1 by PRMT5 is important for its function. Thus, we propose that PRMT5 loss leads to cell death, at least in part, by affecting the function of SRSF1.

PRMT5 depletion affects the binding of SRSF1 to mRNAs and proteins

The same three amino acids in SRSF1 (R93, R97 and R109) were previously shown to be important for its proper cellular localization and activity[37]. However, SRSF1 localization was affected only upon mutating these sites to alanines and not lysines, suggesting the importance of positive charge rather than methylation[37]. To analyze this in THP-1 cells, we performed nuclear-cytoplasm fractionation with and without PRMT5 and compared the amounts of SRSF1 in different fractions. As a result, we did not observe a change in SRSF1 localization after *PRMT5* knockdown (Extended Data Fig.6a, b). We also performed experiments in HeLa cells, similar to the ones presented in Sinha et al.[37], and found that when triple-flag-tagged wild type SRSF1, triple R-to-K or triple R-to-A SRSF1 mutants were mildly overexpressed, all three demonstrate predominantly nuclear localization (Extended Data Fig.6c). Some localization changes of the mutants could be observed only upon increased overexpression (Extended Data Fig.6d). Since mutant SRSF1 relocalization occurs only at high overexpression levels and mostly for the triple R-to-A mutant, it is unlikely that the primary effect of SRSF1 methylation is to retain it in the nucleus.

To further investigate the effect of PRMT5 on SRSF1 function we analyzed changes in SRSF1-bound mRNAs and proteins upon PRMT5 depletion. First, we performed SRSF1 RNA-immunoprecipitation (RIP) in cells transduced with either a negative control sgRNA or sgRNAs against *PRMT5* or *SRSF1*. Efficient immunoprecipitation was verified by western blotting (Extended Data Fig.7a). *SRSF1* KD samples did not yield detectable RNA amounts after RIP, in contrast to negative control and *PRMT5* KD samples, indicating highly specific immunoprecipitation (Extended Data Fig.7b). Next-generation sequencing of the pulled down RNA reliably quantified mRNAs of 13754 genes, of which 4459 were significantly differentially bound between the negative control and *PRMT5* KD conditions (q-value < 0.05) (Fig.7a, Supplementary Table 3). There was a clear and significant enrichment of the differentially spliced genes among the genes which mRNAs were differentially bound by SRSF1 upon *PRMT5* KD (chi-square p-value = 2.2e-16) (Fig.7b, c), suggesting that alternative splicing of these is caused by altered interaction with SRSF1. As an example, five out of seven essential alternatively spliced genes described above (*FDPS*, *POLD1*, *PNISR*, *PNKP*, *POLD2*) were differentially bound by SRSF1, with four out five losing SRSF1 binding (Fig.7a).

Since arginine methylation is known to regulate protein-protein interactions, we performed SRSF1 IP-MS interactomics in cells with and without PRMT5. This approach identified 350 specific SRSF1 interactors (significantly enriched over an IgG control, q-value < 0.05). The identified interactors were enriched in proteins involved in regulating mRNA splicing, RNA transport, transcription and translation (Supplementary Table 4), consistently with previous reports on SRSF1 involvement in these processes[38–40]. Of the 350 binding partners, 162 were differentially bound to SRSF1 between the two conditions (at least 2-fold change, q-value < 0.05) (Fig. 7d). Interestingly, the majority of the SRSF1 interactors showed

decreased abundance in the *PRMT5* KD affinity purification, suggesting that arginine methylation promotes the interaction of SRSF1 with other proteins. The decreased interactors were enriched for proteins involved in mRNA splicing, secondary structure unwinding and transport, while increased SRSF1 binding was observed for multiple ribosomal proteins (Table 2,3). Such differential binding pattern indicates redistribution of SRSF1 between various cellular processes upon *PRMT5* KD and likely contributes to differential splicing and cell death phenotype upon PRMT5 depletion (Fig.7e).

The SRSF1 IP-MS also allowed more extensive arginine methylation analysis of the SRSF1 protein. Arginine methylation was detected on the same sites as in the global arginine methylation profiling approach (R93, R97 and R109), and all the 9 identified peptides covering these sites demonstrated decreased abundance upon *PRMT5* KD (Extended Data Fig. 7c). While both mono- and dimethylation were detected for positions R93 and R109, only dimethylated R97 was identified.

In summary, we found that PRMT5 depletion leads to decreased arginine methylation of SRSF1 and extensive changes in its binding to mRNA and proteins.

Discussion

Here we demonstrated the requirement of the catalytic activity of PRMT5 for the growth of the human AML cells bearing the MLL-AF9 rearrangement. This is consistent with the previous observations in a mouse model of this leukemia type, where *Prmt5* knockout or chemical inhibition decreased leukemia burden and prolonged animal survival[41]. Together, these suggest PRMT5 inhibition as a potential therapeutic approach in AML, and it would be interesting to investigate whether AML patients with mutations in spliceosome proteins are particularly sensitive to PRMT5 inhibition.

In this study, we performed large-scale identification of PRMT5 substrates. In a recent resource paper[42], which was published while this manuscript was prepared for submission, a number of novel PRMT5 substrates were identified in HeLa cells. This study employed a SILAC method (MS1-based quantitation) with two biological replicates. Many of the substrates identified by Musiani et al.[42] were also identified and confirmed by in vitro methylation in our report (e.g. WDR33, SNRPB and others). While Musiani et al. also identified SRSF1 methylated peptides, SRSF1 was not confirmed as a substrate, since the peptides were only identified in one of the replicates, which prohibited statistical analysis. This reflects a limitation of SILAC quantitation in comparison with the TMT approach, which is more sensitive and allows for more robust statistical treatment[43].

We specifically focused on the identified PRMT5 substrates, which are essential for the proliferation of AML cells, since those are most likely to be downstream of PRMT5 in conferring cell survival. Our validation and rescue experiments confirmed SRSF1 as a direct PRMT5 target and demonstrated the importance of methylation for its function.

SRSF1 belongs to the family of serine/arginine-rich splicing factors. It is known to shuttle between the cytoplasm and the nucleus[44], where it binds to exonic splicing enhancers and stimulates splicing[45–47]. In addition, SRSF1 is involved in other processes, including

nonsense-mediated mRNA decay, translation and mRNA transport[38–40]. SRSF1 is overexpressed in multiple cancers and has known oncogenic properties[48]. Posttranslational modifications play an important role in the function of SRSF1. Particularly, phosphorylation of SRSF1 in the RS domain is required for its transport to the nucleus and localization to the sites of splicing[49,50]. The three arginines in SRSF1 that we identified as targeted by PRMT5 were previously shown to regulate correct localization and function of SRSF1[37]. We have not observed major changes in SRSF1 localization when the methylated arginines were changed to lysines or alanines or when PRMT5 was depleted. Instead, we found that *PRMT5* KD induces disruption of the SRSF1 interaction network and extensive changes in the repertoire of mRNAs bound to it. Since all three PRMT5-methylated residues are located in the glycine-rich hinge connecting the two RNA recognition motifs of SRSF1, it is possible that loss of methylation in this region largely affects the protein structure. Taken together, our results suggest that SRSF1 is a key substrate for PRMT5, which can explain why PRMT5 is essential for leukemia cells and also, potentially, other types of cancers.

Interestingly, we did not observe extensive changes in total mRNA levels for the majority of the genes differentially spliced upon PRMT5 depletion. However, decreased protein expression was observed for some of them. Alternative splicing in such cases could lead to mRNA retention in the nucleus, also known as intron detention[51,52], inefficient translation of the alternatively spliced mRNAs[52,53] or instability of the resulting protein isoforms. This agrees with the report by Braun et al., which demonstrated increased intron detention in PRMT5 inhibitor-treated glioma cells[22]. We found further similarities between the alternative splicing events induced by PRMT5 loss in human AML and glioma cells, suggesting common mechanisms of PRMT5 function. We found several essential genes that exhibit changes in splicing and a concomitant downregulation on protein level. These most likely explain the cell death phenotype upon PRMT5 downregulation. It could be interesting to test whether chemical targeting of these essential proteins could synergize with PRMT5 inhibition in impeding cancer cell proliferation.

Surprisingly, for the majority of the identified essential substrates R-to-K mutants were functional in our rescue assays. However, we found that PRMT5 often methylates several proteins in the same pathway or complex, e.g. SNRPB and SNRPN, CCT7 and CCT4, PABPC4 and PABPN1. This could suggest functional redundancy and requirement to mutate to all of them to see an effect. Therefore, strong proliferation defect we observe upon PRMT5 depletion likely represents a combined phenotype from affecting multiple cellular processes. Despite the complexity of the PRMT5 functions, the comprehensive list of substrates we report could be used to identify additional pathways to target in cancer. One of the current clinical trials with the PRMT5 inhibitor () is using SDMA plasma levels as a readout of treatment efficacy. It would be interesting to investigate if the validated essential substrates could be used as more specific biomarkers for PRMT5 activity and treatment response.

In summary, this study provides a comprehensive resource of PRMT5 substrates in human acute myeloid leukemia and directly links the alterations in splicing patterns and cell death upon PRMT5 depletion to the arginine methylation of the splicing factor SRSF1.

Methods

Plasmids, sgRNA cloning and site-directed mutagenesis

pHR-SFFV-KRAB-dCas9–2A-CHERRY, pLentiCas9-blast, pU6-sgRNA-EF1α-puro-T2A-BFP, pLenti PGK Hygro dest and pLEX_307 were purchased from Addgene (cat.no 60954, 60955, 52962, 41392 and 19066), PB-CAG-hph-dest was a kind gift from José Silva. For sgRNA cloning, oligos were annealed in annealing buffer (200 mM potassium acetate, 60 mM HEPES-KOH pH 7.4, 4 mM magnesium acetate) and ligated into BstXI+BlpI digested pU6-sgRNA-EF1α-puro-T2A-BFP. Site-directed mutagenesis was performed using QuickChange Lightning Multi Site-Directed Mutagenesis Kit (Agilent) or Q5® Site-Directed Mutagenesis Kit (NEB).

sgRNA design

CRISPRko sgRNAs were designed using the sgRNA Designer: CRISPRko – Broad Institute (https://portals.broadinstitute.org/gpp/public/analysis-tools/sgrna-design). CRISPRi sgRNAs were designed as described previously[54]. Supplementary Table 5 contains sequences of all the sgRNAs used in the study.

Cell lines and cell culture

THP-1 were obtained from ATCC, MOLM-13 and MONOMAC6 - from DSMZ, HeLa cells were a kind gift from the Xuejun Jiang Lab. All the cells used in the study were mycoplasma negative, no cell authentication was performed. HEK293FT packaging cells and HeLa cells were cultured in DMEM, high glucose, GlutaMAX supplement, pyruvate medium (Thermo Fisher SCIENTIFIC) containing 10% heat-inactivated FCS (HyClone) and 1x Penicillin and Streptomycin (Thermo Fisher SCIENTIFIC). THP-1 monocytic leukemia cells were cultured in RPMI 1640, GlutaMAX supplement medium (Thermo Fisher SCIENTIFIC) containing 10% heat-inactivated FCS (HyClone) and 1x Penicillin and Streptomycin (Thermo Fisher SCIENTIFIC). MOLM-13 and MONOMAC-6 monocytic leukemia cells were cultured in RPMI 1640, GlutaMAX supplement medium (Thermo Fisher SCIENTIFIC) containing 20% heat-inactivated FCS (SIGMA-ALDRICH), 1x NEAA (Gibco), 1x sodium pyruvate (Gibco) and 1x Penicillin and Streptomycin (Thermo Fisher SCIENTIFIC). For MONOMAC-6 human insulin was added to the culture medium at the concentration of 10 μg/ml. Mouse MLL-AF9 secondary leukemia cells were generated in house and were cultured in RPMI 1640, GlutaMAX supplement medium (Thermo Fisher SCIENTIFIC) containing 20% heat-inactivated FCS (HyClone), 1x Penicillin and Streptomycin (Thermo Fisher SCIENTIFIC) and 20% of culture media supernatant from the IL-3-secreting cell line (homemade).

Western blotting

The following primary and secondary antibodies were used: PRMT5 (Abcam, ab109451), Vinculin (Sigma, SAB4200080), SDMA (Cell Signalling, 13222), GAPDH (Abcam, ab181602), SRSF1 (Abcam, ab38017), Lamin B1 (Abcam, ab16048), b-Actin (Abcam, ab6276), peroxidase-labelled anti-mouse and anti-rabbit IgG (Vector Laboratories), IRDye® 800CW Goat anti-Rabbit IgG and IRDye® 680RD Goat anti-Mouse IgG (LI-COR). Western

blotting quantification was performed using Image Studio Lite software (Li-COR Biosciences).

Nuclear-cytoplasm fractionation

20 million cells were lysed in 1.3 ml of ice-cold lysis buffer (10 mM Tris-HCl, pH 7.9; 10 mM KCl; 1.5 mM MgCl2; protease inhibitor cocktail) and span down at 400 g for 5 min at 4 degrees C. The pellet was resuspended in 600 μl of ice-cold lysis buffer + 0.2% NP-40 and precipitated at 3300 g for 15 min at 4 degrees C. The resulting supernatant was collected as the cytoplasmic fraction. The pellet was washed with 3 ml of ice-cold PBS and precipipated at 3300 g for 5 min at 4 degrees C. The resulting pellet was resuspended in TOPEX+ buffer (300 mM NaCl; 50 mM Tris-HCl, pH 7.5; 0.5% Triton X-100; 1% SDS; 1 mM DTT; 33 U/ml Benzonase (Novagen, 70664); protease inhibitor cocktail) and collected as a nuclear fraction.

Cell transfection

Lipofection of HeLa cells was performed using Lipofectamin 2000 (Thermo Fisher Scientific) according to manufacturer's instructions.

Immunofluorescence

HeLa cells were plated on glass slides a day after transfection and immunostained the next day as follows: fixed in 4% PFA for 15 min, permeabilized in 0.5% Triton X-100 in PBS for 10 min, blocked in 0.1% Triton X-100 in PBS with goat serum (1:80) for 30 min, stained with primary antibody in 0.1% Triton X-100 in PBS with goat serum (1:100) for 1 hour at 37 degrees C, washed three times in 0.1% Triton X-100 in PBS for 5 min, stained with secondary antibody in 0.1% Triton X-100 in PBS for 1 hour, washed three times in 0.1% Triton X-100 in PBS for 5 min, mounted in Vectashield mounting media (VECTOR) with DAPI. Antibodies used: SRSF1 (1:500, Abcam, ab38017), FLAG (1:500, Sigma, F1804), Alexa Flour 488 goat anti-rabbit IgG and Alexa Flour 594 goat anti-mouse IgG (1:500, Thermo Fisher Scientific). Leica TCS SP5-II confocal microscope on inverted stand, with 63x/1.4 NA oil objective, was used to take single optical slices in DAPI, Alexa488 and Alexa594 channels.

Flow cytometry

Flow cytometry was performed using a BD LSR II flow cytometer, BD FACSAria III Cell Sorter and Beckman Coulter CytoFlex.

Virus production and lentiviral transduction

HEK293FT cells were co-transfected with a construct of interest and pAX8 and pCMV-VSV using a standard calcium phosphate protocol. The viral supernatant was collected 72 hours after HEK293FT transfection and used for transduction. All the leukemia cells were transduced using a RetroNectin Bound Virus Infection Method (TaKaRa) according to the manufacturer's instructions. Transduction was performed in presence of polybrene at 8 μg/ml. Antibiotic selection was added 24 hours after transduction.

RNA extraction, cDNA synthesis and qRT-PCR analysis

Total RNA was extracted using RNeasy Plus Mini Kit (Qiagen) in accordance with the manufacturer's protocol. One microgram of total RNA was subjected to reverse transcription using Transcriptor Universal cDNA Master (Roche). Quantitative PCR with reverse transcription (qRT-PCR) reactions were set up in triplicate using LightCycler 480 SYBR Green I Master (Roche) and primers listed in Supplementary Table 6. qRT-PCR experiments were performed on a LightCycler 480 Instrument II (Roche). Unless stated otherwise, relative quantitation was performed using a standard curve and the obtained values were normalized to RPLP0 expression. For the validation of differential splicing events, the values obtained for a differential event were divided on the values for the constitutive splicing event of the same gene.

Growth curves and competition assays

For the growth curve experiments, the cells were collected 2 days after the addition of puromycin (3 days post-transduction) and plated at the density of 500,000 cells per well of a 6-well plate. The cells were counted every 72 hours and 500,000 cells were replated for the next timepoint. For the competition assay, the cells were collected 2 days after the addition of puromycin (3 days post-transduction) and were mixed with untransduced cells at approximately 8:1 ratio of transduced to untransduced cells. The percentage of BFP% (transduced) cells was then recorded on a flow cytometer at the specified timepoints.

Rescue experiments

THP-1-wtCas9 or cdCas9-KRAB cells were transduced with the constructs constitutively expressing a wild type or an R-to-K mutant substrate. After selection, the cells were transduced with a corresponding sgRNA and their proliferative capacity measured in a competition assay with untransduced cells using flow cytometry.

RNA-sequencing

RNA was extracted using a Qiagen RNeasy Kit. The libraries were prepared using an Illumina TruSeq v2 kit. The samples were sequenced using NextSeq 500.

Protein extraction and TMT labelling

Five million cells were lysed in 330 μL of ice-cold RIPA buffer with 3 U of Benzonase and protease and phosphatase inhibitors (cOmplete and PhosStop, Roche) using a sonication probe with 5 cycles of 50% amplitude with 5 seconds intervals. Proteins were precipitated by addition of 1.2 ml of ice-cold acetone for 2 hours at −20°C and then pelleted by centrifugation at 20.000 g. The samples were resuspended in 150 μL of the digestion buffer, containing 8M urea, 0.1M HEPES, pH 8.0 using a sonication probe with 5 cycles of 50% amplitude with 5 seconds intervals. Protein concentration was estimated with Pierce™ BCA Protein Assay Kit. An aliquot containing 300 μg of protein material was adjusted to 200 μL with the digestion buffer. Proteins were reduced and alkylated by addition of 10 mM TCEP and 40 mM chloroacetamide and digested with lysC (1:50 protease: protein ratio) at 37°C for 4 hours. The sample was then diluted 8-fold with 0.1 M HEPES, pH 8 buffer and digested with trypsin (1:25 protease:protein ratio) at 37°C overnight. The obtained peptides

were desalted on a 30 mg Oasis HLB cartridge (WAT094225) according to the manufacturer recommendations, vacuum-dried to 2–3 μL volume, evaporated using a vacuum centrifuge with 2 μL of DMSO to prevent complete evaporation and resuspended in TMT labelling buffer (0.1 M HEPES, pH 8). Peptide concentration was measured by Pierce BCA Protein Assay Kit. 60 μg of peptide material for each sample was labelled with 0.5 mg of the TMT labelling reagent according to the manufacturer recommendations. 10 samples labelled by complementary 10plex TMT reagents were pooled for the use in downstream procedures.

Immunoaffinity enrichment of peptides containing mono- and dimethylated arginines

Enrichment was performed using a PTMScan® Mono-Methyl Arginine Motif [mme-RG] Kit #12235 and PTMScan® Symmetric Di-Methyl Arginine Motif [sdme-RG] Kit #13563 according to manufacturer instructions (Cell Signaling Technology). The procedure was first benchmarked against a positive control sample PTMScan® Trypsin Digested Control Peptides I #12219 provided with the kit (number of identified peptides was according to specification, data not shown). The procedure was scaled down to using only 20 μL of beads (1/4 of the volume recommended for one sample) for 600 μg of peptide material in a pooled 10plex TMT sample. To minimize the loss of beads all the washes were performed on the Pierce™ Spin Cups - Cellulose Acetate Filter (#69702).

LC-MS/MS data acquisition and data analysis

The detailed procedures are described in Supplementary Note. Briefly, the data was acquired using MS3 multinotch selection TMT method as described previously[20] on Orbitrap Fusion LUMOS platform. Data was analysed using Proteome Discoverer 2.3 with Mascot 2.3.2 as search engine and ptmRS as PTM localization method. Differential expression test was performed using limma package[55] and p-values were adjusted by Storey method.

In vitro methyltransferase assay

The assay was performed in 50 mM HEPES (pH 8.0), 50 mM NaCl, 1 mM EDTA, 5mM DTT and 0.2mM SAM. Each reaction was performed in 25 μL for 12 hours at 37°C with 300 ng of the corresponding peptide and 0.2 μL of active human recombinant PRMT5-MEP50 complex (Sigma, SRP0145) or water (negative control). The product of the reaction was desalted on a stageTip with 100 μL of 0.1% TFA and eluted in 30 μL of 50% ACN 0.1% FA. 2 μL of the desalted product was directly infused into LTQ Orbitrap XL using nanoAcquity UPLC (Waters) and analyzed at 100K resolution. The data was deconvoluted with Xtract with SN threshold 10, spectra extracted from the .xml outputs and plotted with the ggplot2 R package.

Defining PRMT5 methylation motif

PRMT5 methylation motif was predicted using the iceLogo online tool (https://iomics.ugent.be/icelogoserver/). 20 amino acid sequences with the arginine modification site in the center were compared to the Swiss-Prot human proteome reference set.

SRSF1 RNA immunoprecipitation and sequencing

The cells were transduced with either a negative control sgRNA or sgRNAs inducing knockdown of *PRMT5* or *SRSF1*. For each condition 3 biological replicates of 20 million cells were collected 6 days after transduction and subjected to RNA immunoprecipitation protocol using Magna RIP™ Kit (Millipore) according to manufacturer's instructions. The immunoprecipitation was performed with 5 μg of anti-SRSF1 antibody 96 (Santa Cruz). The obtained RNA was used for the preparation of sequencing libraries using the TruSeq RNA Library Prep Kit v2, starting at the Elute, Prime, Fragment step. The details of the RIP-sequencing data analysis can be found in the Supplementary Note.

SRSF1 interactomics analysis

The cells were lysed in lysis buffer (50 mM EPPS, pH 7.4, 150 mM NaCl, 1 mM EDTA, 1% Triton X-100, protease inhibitors), briefly sonicated, cleared from cell debris, pre-cleared with protein A Sepharose beads and immunoprecipitated with anti-SRSF1 antibody 96 (Santa Cruz) and protein A Sepharose beads. After immunoprecipitation, the beads were washed five times in wash buffer (50 mM EPPS, pH 7.4, 150 mM NaCl) and subjected to trypsin digestion overnight at 37C (20 mM EPPS pH 8.5, 5 mM TCEP, 20 mM chloracetamide, 10 ng/μl LysC and 20 ng/μl Trypsin). The digest was labelled with 20 g/L TMT tags, as recommended by the manufacturer, and half of the material was fractionated by Pierce™ High pH Reversed-Phase Peptide Fractionation Kit concatenating 2 fractions into a superfraction (e.g. 1 and 5). After desalting the samples were evaporated using vacuum centrifugespeedvaced, resuspended in 0.1% TFA and analyzed by LC-MS/MS.

Emetine treatment

The cells were transduced with either a negative control or a PRMT5 sgRNA and cultured for 6 days. After that either water or emetine (at a final concentration of 100 μg/ml) were added for 3 hours. The cells were harvested and analyzed by qRT-PCR.

Reporting Summary statement

Further information on experimental design is available in the Nature Research Reporting Summary linked to this article.

Code availability

GitHub project with the RNA-sequencing analysis code is available at: https://github.com/VGrinev/transcriptome-analysis/blob/master/TranscriptsFeatures. Any additional code will be provided upon request.

Data availability

Next-generation sequencing has been submitted to GEO (accession number: GSE129652). Proteomics data has been submitted to ProteomeXchange (accession number: PXD013611). Source data for all the main Figures and Extended Data Figures 1, 2, 4, 6, 7 are available with the paper online either as Source Data or in Supplementary Tables. All other data will be made available on request.

Extended Data

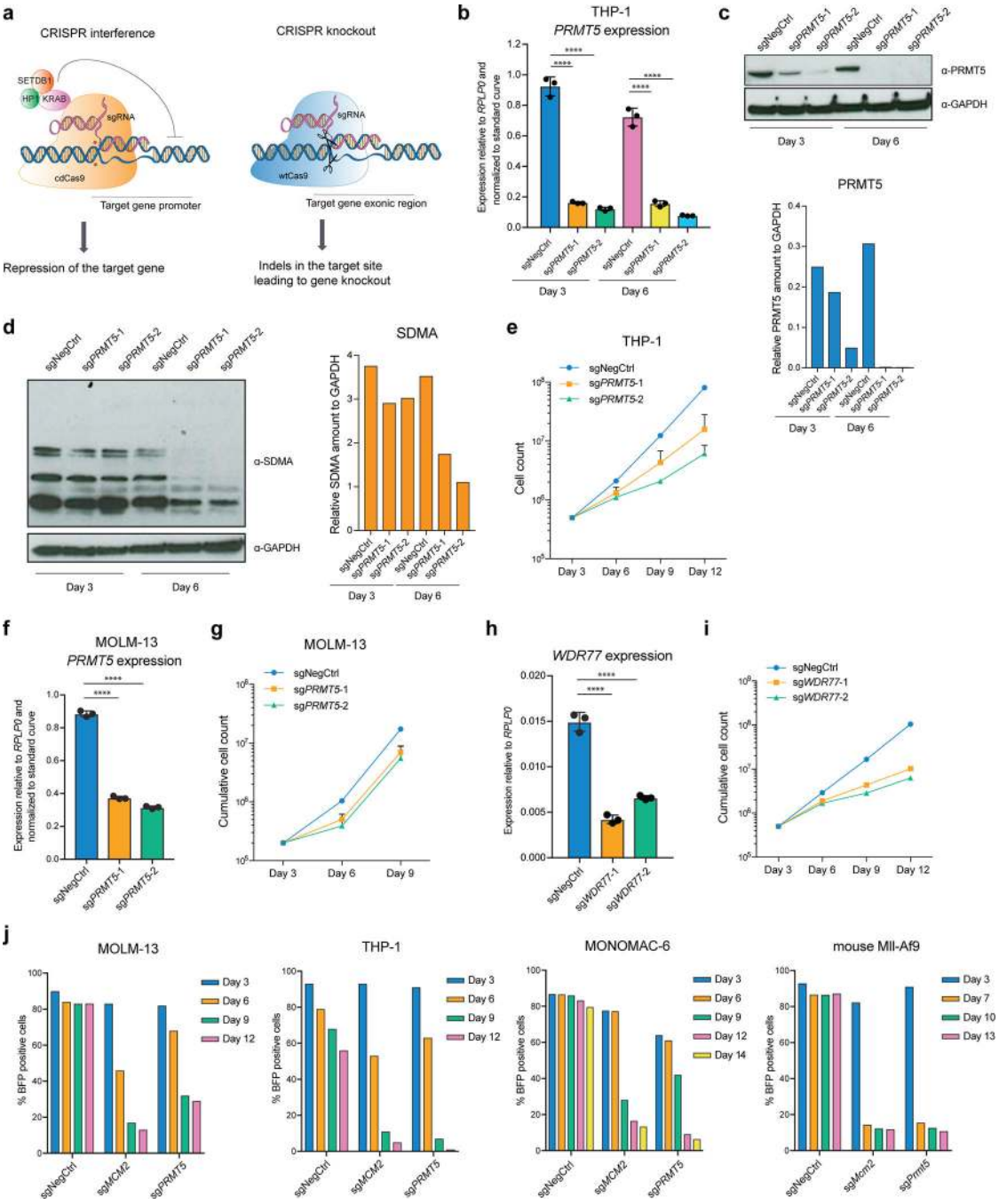

Extended Data Fig. 1. PRMT5 and WDR77 are required for the survival of mouse and human AML cells.

a, Overview of the CRISPR interference and knockout approaches. **b,** qRT-PCR analysis of *PRMT5* expression in THP-1-cdCas9-KRAB cells transduced with a non-targeting (NegCtrl) sgRNA or two sgRNAs targeting *PRMT5* (3 and 6 days post-transduction). The values are normalized to *RPLP0* and shown as mean ±SD (n=3, **** is p-value < 0.0001 using Sidak's multiple comparisons test). **c-d,** Western blot analysis of PRMT5 and GAPDH (**c**) and symmetrical arginine dimethylation (SDMA) (**d**) levels in THP-1-cdCas9-KRAB

cells transduced with a non-targeting sgRNA or two sgRNAs targeting *PRMT5* (3 and 6 days post-transduction). Bar charts show quantification of protein levels relative to a loading control. **e,** Growth curves of THP-1-cdCas9-KRAB cells transduced with a non-targeting sgRNA or two sgRNAs targeting *PRMT5*. Here and below, X-axis indicates number of days after transduction. **f,** qRT-PCR analysis of *PRMT5* expression in MOLM-13-cdCas9-KRAB cells transduced with a non-targeting sgRNA or two sgRNAs targeting *PRMT5* (3 and 6 days post-transduction). The values are normalized to *RPLP0* and shown as mean ±SD (n=3, **** is p-value < 0.0001 using Sidak's multiple comparisons test). **g,** Growth curves of MOLM-13-cdCas9-KRAB cells transduced with a non-targeting sgRNA or two sgRNAs targeting *PRMT5*. **h**, qRT-PCR analysis of *PRMT5* expression in THP-1-cdCas9-KRAB cells transduced with a non-targeting sgRNA or two sgRNAs targeting *WDR77* (3 and 6 days post-transduction). The values are normalized to *RPLP0* and shown as mean ±SD (n=3, **** is p-value < 0.0001 using Sidak's multiple comparisons test). **i)** Growth curves of THP-1-cdCas9-KRAB cells transduced with a non-targeting sgRNA or two sgRNAs targeting *WDR77*. **j,** Competition assays of THP-1-wtCas9, MOLM-13-wtCas9, MONOMAC-6-wtCas9 and mouse Mll-Af9-wtCas9 cells transduced with a non-targeting sgRNA or sgRNAs targeting *MCM2 (Mcm2)* (positive control) or *PRMT5 (Prmt5)*. The experiments were repeated at least twice with similar results. The uncropped western blots are presented in the Source Data.

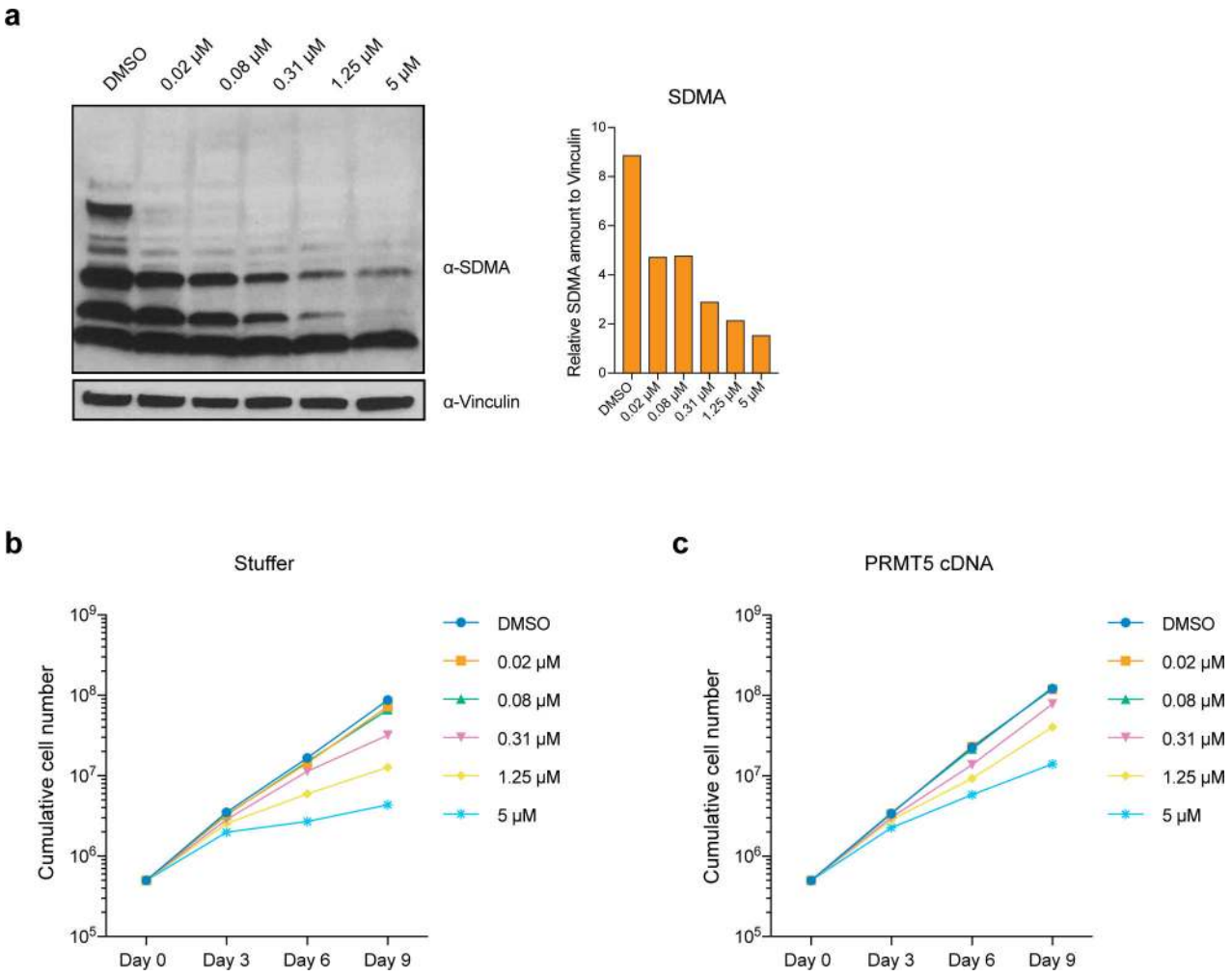

Extended Data Fig. 2. Chemical inhibition of PRMT5 leads to growth defects in AML cells.

a, Western blot analysis of symmetrical arginine dimethylation (SDMA) levels and Vinculin in THP-1 cells treated with DMSO or different doses of PRMT5 inhibitor EPZ015666 at 6 days after the addition of a compound. Bar chart shows quantification of protein levels relative to a loading control. **b,** Growth curves of THP-1-cdCas9-KRAB-stuffer cells treated with DMSO or different doses of PRMT5 inhibitor EPZ015666. X-axis indicates number of days after addition of the compound. **c,** Growth curves of THP-1-cdCas9-KRAB-wtPRMT5 cells treated with DMSO or different doses of PRMT5 inhibitor EPZ015666. X-axis indicates number of days after addition of the compound. The experiments were repeated twice with similar results. The uncropped western blots are available in the Source Data.

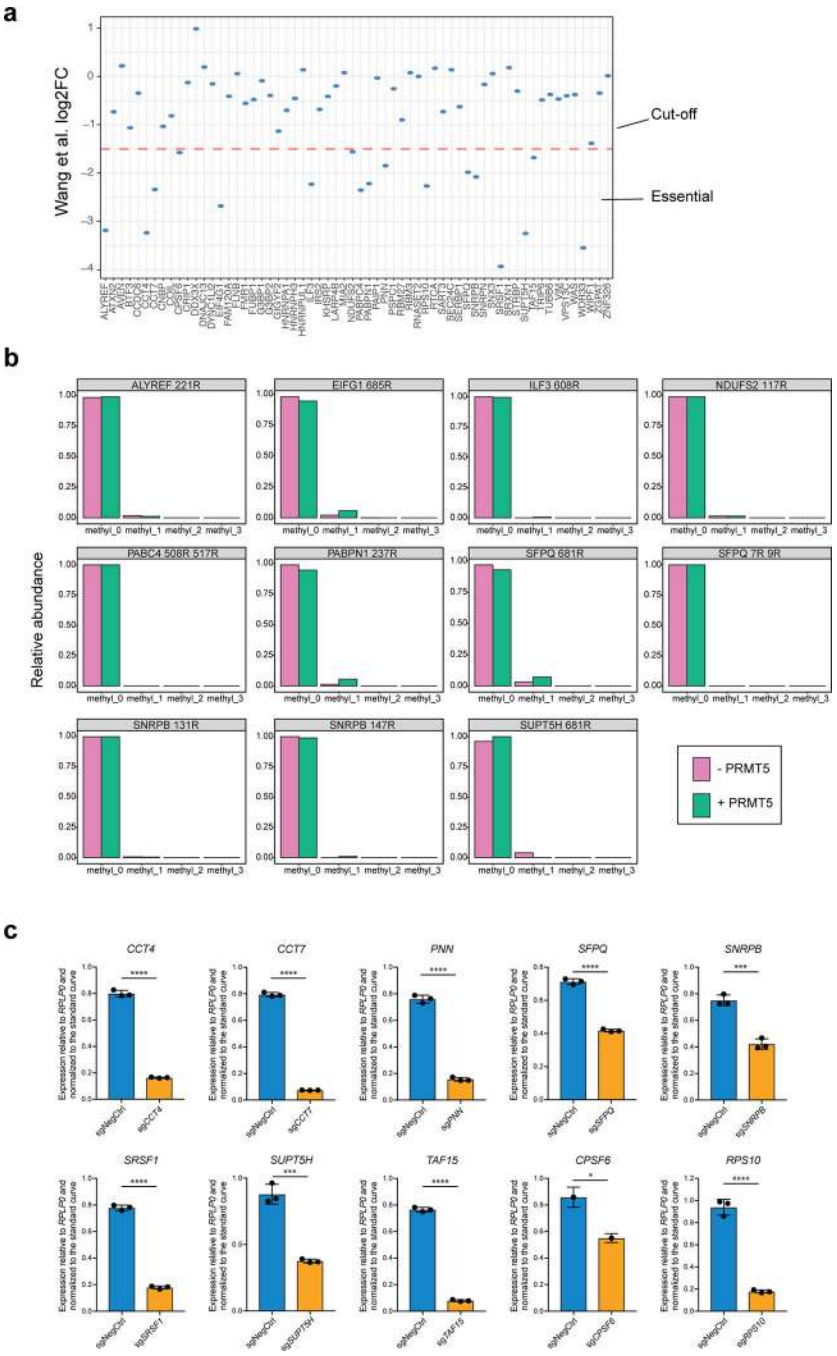

Extended Data Fig. 3. Validation of the essential PRMT5 substrates.

a, 17 out of 62 potential PRMT5 substrates were chosen as potentially essential according to a previously published CRISPRko screen in THP-1 cells. Y axis represents log2FC of the relative abundance of sgRNA in the screen and −1.5 was chosen as a cut-off. **b,** Distributions of relative abundances of unmethylated and methylated peptide forms after the incubation with or without recombinant PRMT5-WDR77 complex. Only the peptides belonging to the unconfirmed PRMT5 substrates are shown here. **c,** qRT-PCR analysis of *CCT4*, *CC7*, *PNN*, *SFPQ*, *SNRPB*, *SRSF1*, *SUPT5H*, *TAF15*, *CPSF6* and *RPS10* expression demonstrates

efficient knockdown of the genes upon CRISPRi sgRNA transduction (n=3, * is p-value < 0.033, *** is p-value < 0.001, **** is p-value < 0.0001 according to the unpaired t test). The experiments were repeated twice with similar results.

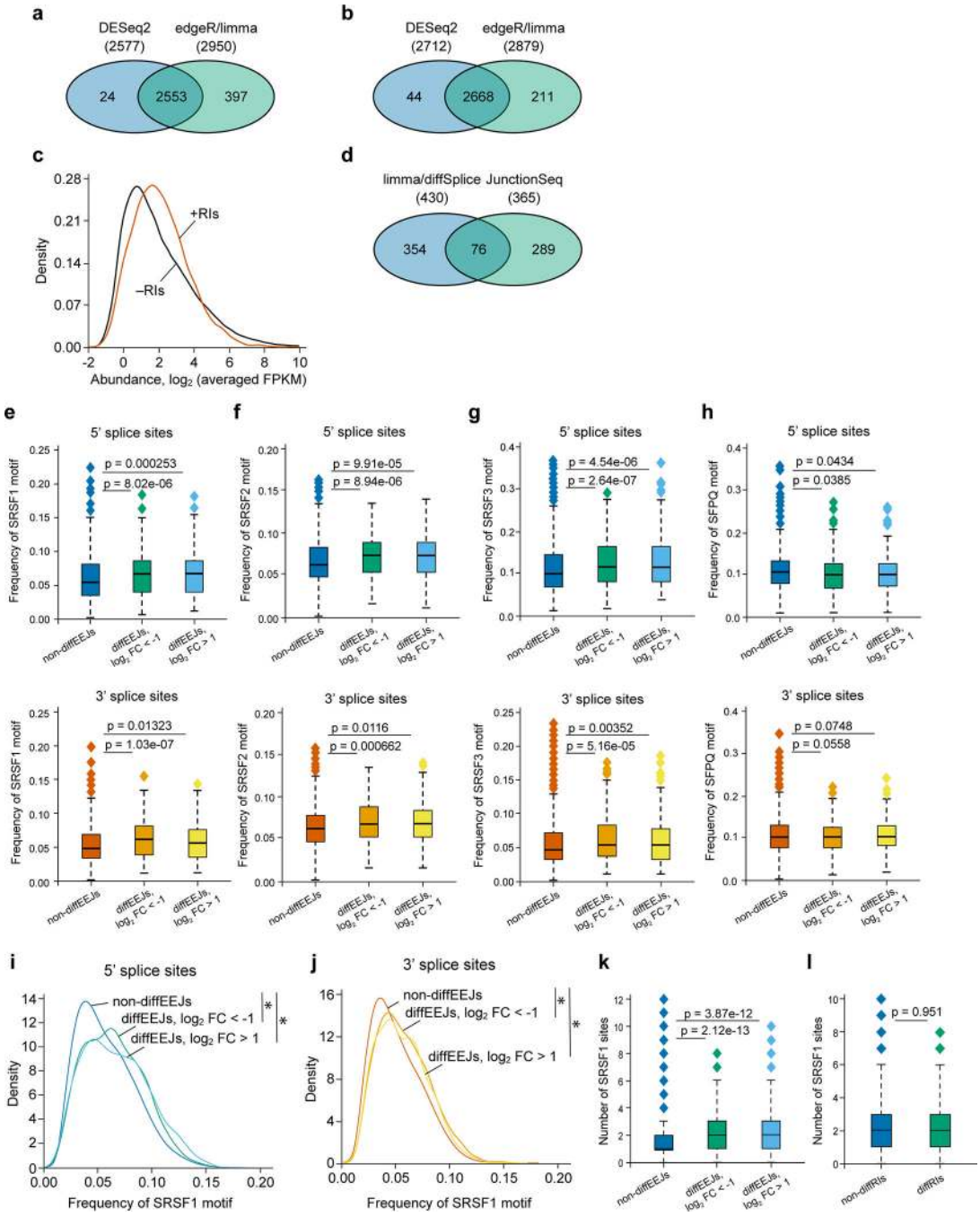

Extended Data Fig. 4. Knockdown of *PRMT5* leads to differential splicing in the transcriptome of THP-1 AML cells.

a, Two independent algorithms (DESeq2 and edgeR-limma) identified 2974 RIs in the transcriptome of THP-1 cells. **b,** In total 2923 of 45450 Cufflinks-assembled transcripts of the THP-1 cells contain DESeq2- or edgeR-limma-detected RIs. Of these, 2668 transcripts are common between the two algorithms. **c,** Density plot of the transcript abundance demonstrating that the transcripts with RIs (+RIs) are highly expressed in the transcriptome of THP-1 cells comparing to RI-free (–RIs) ones. **d,** The knockdown of *PRMT5* leads to

differential usage of a subset of EEJs in the transcriptome of THP-1 cells. The differentially used EEJs were determined using two independent algorithms (limma-diffSplice and JunctionSeq) with moderate overlap between the results. **e-g,** SRSF1 (e), SRSF2 (f) and SRSF3 (g) motifs are significantly enriched both at the 5' and 3' splice sites of the differential EEJs (dynamic thresholding). **h,** SFPQ motif is not significantly enriched at the 5' or 3' splice sites of the differential EEJs (dynamic thresholding). **i-j,** Density diagrams of SRSF1 motif frequency at the 5' and 3' splice sites of the differential and non-differential EEJs in U-87 MG cells. Stars indicate statistically significant differences ($p < 0.01$) (dynamic thresholding). **k-l,** Median absolute numbers of SRSF1 motifs in differential and non-differential splicing events in U-87 MG cells (fixed thresholding). Boxplot summary (**e-h, k, l**): outliers (diamonds), minimum (lower whisker), first quartile (lower bound of box), median (horizontal line inside box), third quartile (upper bound of box), interquartile range (box), and maximum (upper whisker).

a

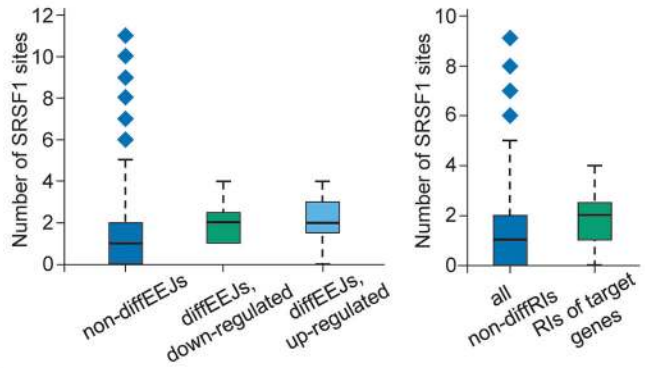

b

Identification of SRSF1 binding sites in the differential splicing events of interest

Type of splicing event	Chromosome	Start	End	Strand	Gene symbol	log_2 FC	p-value	q-value	Number of SRSF1 sites at	
									5' splice sites	3' splice sites
EEJ	chr1	155308965	155310043	+	FDPS	0.49	4.57E-04	5.76E-02	2	1
EEJ	chr1	155308965	155310064	+	FDPS	-0.65	3.42E-05	1.07E-02	2	1
EEJ	chr1	155308965	155312255	+	FDPS	3.26	1.01E-05	4.40E-03	2	1
RI	chr1	155312980	155316862	+	FDPS	0.39	7.77E-05	4.78E-03	3	2
EEJ	chr1	155318332	155318856	+	FDPS	2.33	1.04E-06	6.77E-04	3	3
EEJ	chr1	155319688	155320409	+	FDPS	0.84	2.64E-07	2.33E-04	3	0
RI	chr1	155319689	155319793	+	FDPS	0.61	9.11E-05	5.46E-03	3	3
RI	chr1	155319954	155320158	+	FDPS	0.89	1.54E-10	3.81E-08	1	2
EEJ	chr6	170580105	170583057	-	PDCD2	-0.76	1.95E-04	3.37E-02	4	0
EEJ	chr6	170582265	170583057	-	PDCD2	1.23	1.28E-04	2.53E-02	4	0
RI	chr6	170582266	170582848	-	PDCD2	1.66	3.69E-07	4.44E-05	2	0
RI	chr6	99408272	99409172	-	PNISR	1.89	7.92E-13	3.37E-10	0	5
EEJ	chr6	99409344	99410741	-	PNISR	-0.93	5.08E-04	6.09E-02	1	2
RI	chr6	99409345	99410740	-	PNISR	0.92	4.52E-07	5.33E-05	1	2
RI	chr6	99410993	99411735	-	PNISR	0.89	4.72E-08	6.98E-06	2	0
EEJ	chr6	99412318	99412551	-	PNISR	1.62	2.99E-08	3.88E-05	0	1
EEJ	chr19	49864071	49864179	-	PNKP	-2.07	1.19E-03	2.68E-02	3	5
RI	chr19	49864237	49864323	-	PNKP	2.73	6.61E-09	1.16E-06	2	2
EEJ	chr19	50415826	50416396	+	POLD1	-0.72	5.43E-04	6.38E-02	2	1
RI	chr19	50415827	50416312	+	POLD1	2.16	1.76E-21	3.34E-18	2	1
RI	chr19	50416724	50416952	+	POLD1	1.99	8.68E-11	2.32E-08	2	4
RI	chr7	44116273	44116429	-	POLD2	2.32	2.18E-12	8.32E-10	1	1
EEJ	chr2	241166441	241167045	+	PPP1R7	1.08	3.31E-05	1.05E-02	1	4
EEJ	chr2	241166441	241169781	+	PPP1R7	-1.15	1.21E-08	1.85E-05	1	2
EEJ	chr2	241169867	241182647	+	PPP1R7	-1.03	6.71E-08	7.66E-05	1	1
RI	chr2	241183025	241183378	+	PPP1R7	-0.81	3.78E-04	1.82E-02	4	2

Extended Data Fig. 5. SRSF1 motif number is increased around the differential splicing sites of the selected essential candidate genes.

a, Median absolute numbers of SRSF1 motifs near all the splicing sites that do not change upon PRMT5 depletion and near the splicing sites that change upon *PRMT5* KD in the selected essential candidate genes (*FDPS*, *PDCD2*, *PNISR*, *PNKP*, *POLD1*, *POLD2*, *PPP1R7*) (fixed thresholding). Boxplot summary: outliers (diamonds), minimum (lower whisker), first quartile (lower bound of box), median (horizontal line inside box), third quartile (upper bound of box), interquartile range (box), and maximum (upper whisker). **b,** Table summary of the identified SRSF1 binding sites in all the splicing events that change upon *PRMT5* KD in the *FDPS*, *PDCD2*, *PNISR*, *PNKP*, *POLD1*, *POLD2*, *PPP1R7* genes.

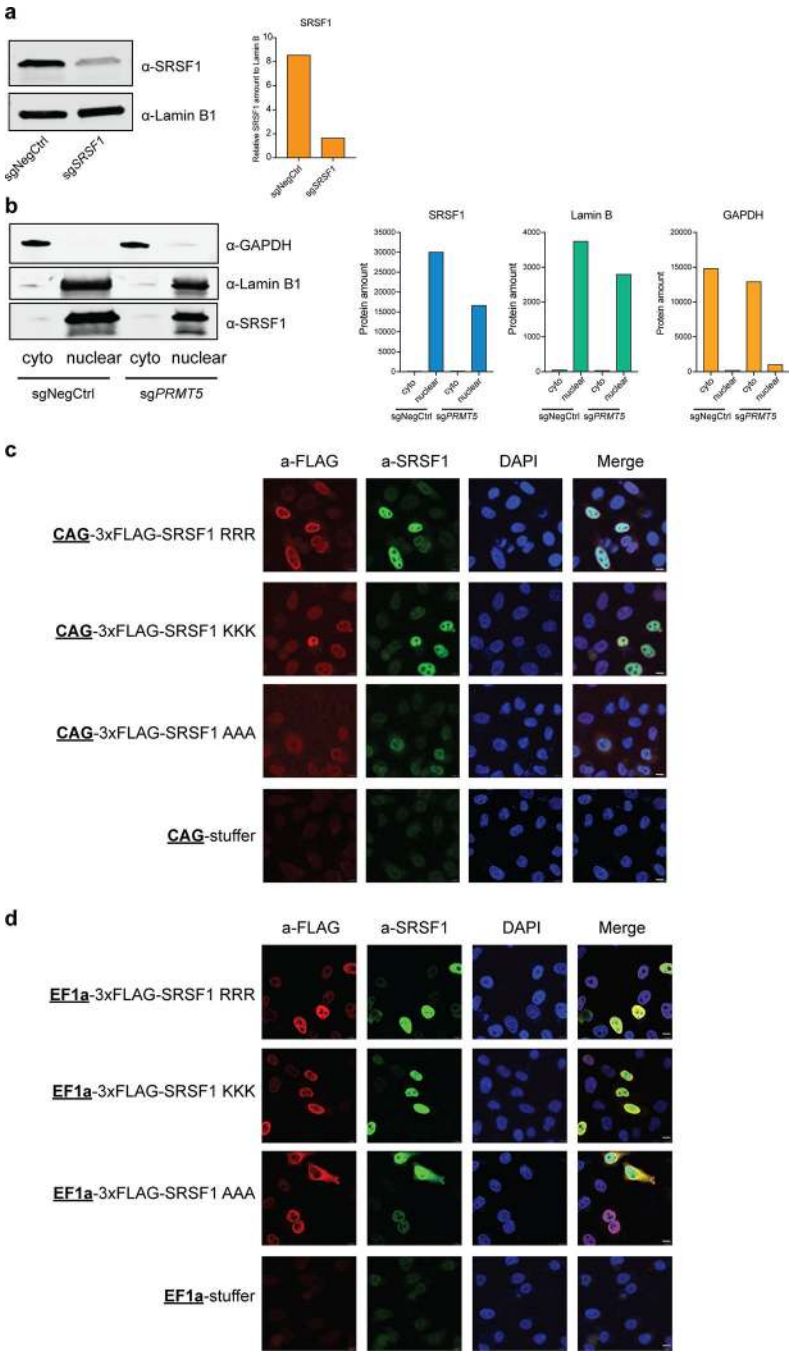

Extended Data Fig. 6. PRMT5 depletion doesn't demonstrate detectable effects on SRSF1 cellular localization.

a, Western blot validation of SRSF1 antibody. Significant decrease in the signal observed after the *SRSF1* knockdown, demonstrating antibody specificity. Bar chart shows quantification of protein levels relative to a loading control. **b,** Western blotting for SRSF1, Lamin B1 and GAPDH after cell transduction with either a negative control or a *PRMT5* sgRNA and subsequent nuclear-cytoplasm fractionation. Lamin B1 and GAPDH were used as controls for successful fractionation into nuclear and cytoplasmic (cyto) fractions,

respectively. Bar chart shows quantification of protein levels. **c,** Representative immunofluorescence images of HeLa cells transiently transfected with either triple-FLAG-tagged wild type, triple R-to-K or triple R-to-A mutant SRSF1 cDNAs driven by the CAG promoter. Scale bar = 10 μm. **d,** Representative immunofluorescence images of HeLa cells transiently transfected with either triple-FLAG-tagged wild type, triple R-to-K or triple R-to-A mutant SRSF1 cDNAs driven by the EF1a promoter. Scale bar = 10 μm. The experiments in the figure were repeated at least twice with similar results. The uncropped western blots are available in the Source Data.

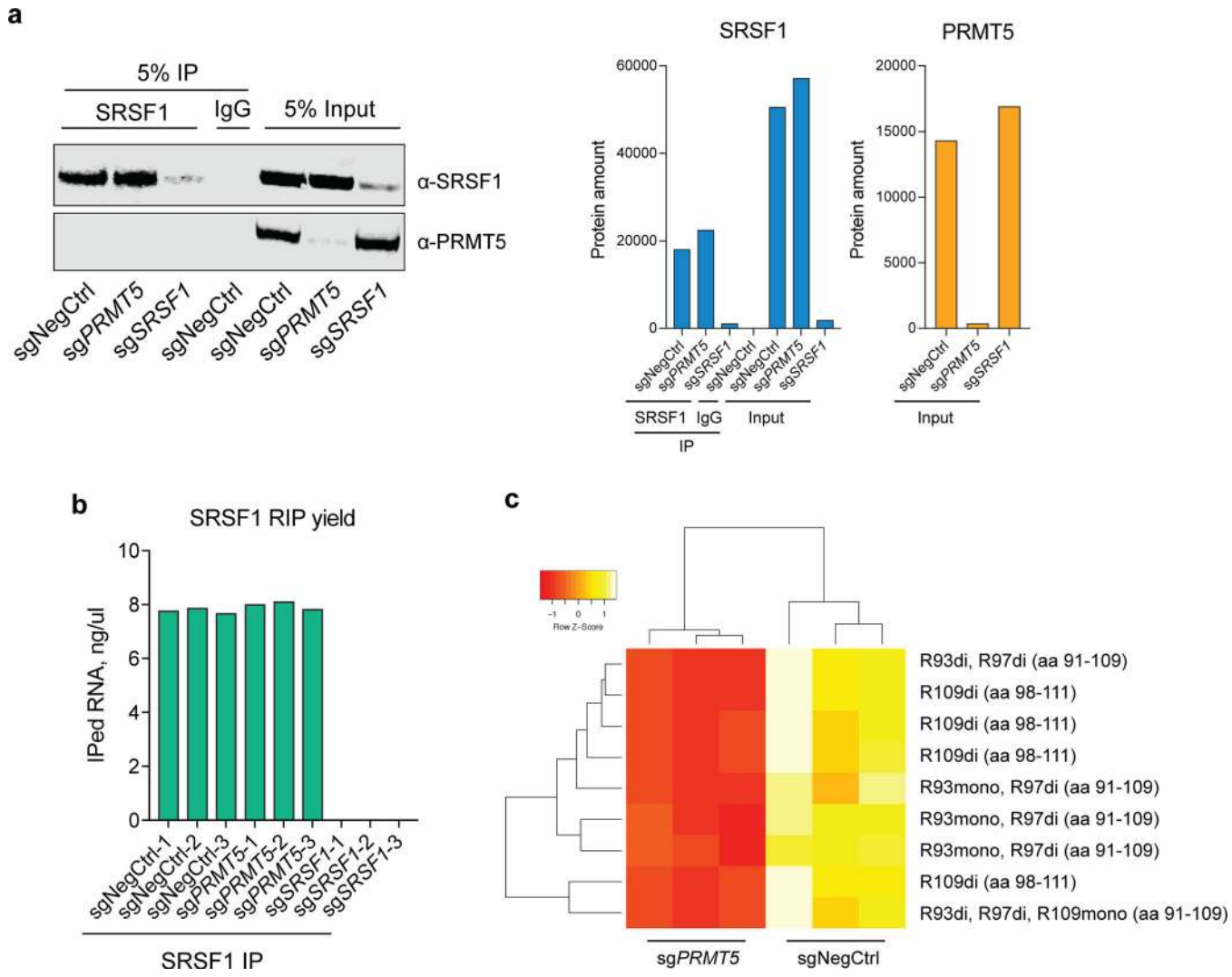

Extended Data Fig. 7. PRMT5 depletion affects the binding of SRSF1 to mRNA and proteins.

a, Western blotting for SRSF1 and PRMT5 in the input and immunoprecipitation samples (either SRSF1 or IgG). Bar chart shows quantification of protein levels. **b,** RNA yield after RNA-immunoprecipitation and purification in three biological replicates of each sample. **c,** Heatmap of the methylated peptides identified for SRSF1 in the negative control and *PRMT5* KD SRSF1 IP-MS samples. "aa" stands for amino acid. Each IP was performed in three biological replicates. The uncropped western blots are available in the Source Data.

Supplementary Material

Refer to Web version on PubMed Central for supplementary material.

Acknowledgments

We thank members of the Helin laboratory for discussions, Sarah Teed and Helene Damhofer for technical assistance, Itys Comet for advice on nuclear-cytoplasm fractionation, Sho Fujisawa and the rest of the Molecular Cytology Core at the MSKCC for microscopy assistance. A.R. and D.S. were funded by the European Union's Horizon 2020 research and innovation programme under the Marie Sklodowska-Curie grant agreements 659171

and 749362, respectively. The work in the Helin laboratory was supported by the Danish Cancer Society (R167-A10877), through a center grant from the NNF to the NNF Center for Stem Cell Biology (NNF17CC0027852), and through the Memorial Sloan Kettering Cancer Center Support Grant (NIH P30 CA008748). Experimental and computational proteomics work at SDU (P.S., V.G., S.K. and O.N.J) was supported by the research infrastructure provided by the Danish National Mass Spectrometry Platform for Functional Proteomics (PRO-MS, 5072–00007B) and VILLUM Center for Bioanalytical Sciences (7292). P.S. was supported by a postdoctoral fellowship from the Lundbeck Foundation (R231–2016-3093). S.K. was supported by a research grant from Independent Research Fund Denmark (to O.N.J., 4181–00172B). Research in the V.G. laboratory was supported in part by the Ministry of Education of the Republic of Belarus, grant #3.08.3 (469/54).

References

1. Larsen SC et al. Proteome-wide analysis of arginine monomethylation reveals widespread occurrence in human cells. Sci Signal 9, rs9–rs9 (2016). [PubMed: 27577262]
2. Blanc RS & Richard S Arginine Methylation: The Coming of Age. Mol. Cell 65, 8–24 (2017). [PubMed: 28061334]
3. Gayatri S & Bedford MT Readers of histone methylarginine marks. Biochim. Biophys. Acta 1839, 702–710 (2014). [PubMed: 24583552]
4. Li X, Wang C, Jiang H & Luo C A patent review of arginine methyltransferase inhibitors (2010–2018). Expert Opin Ther Pat 29, 97–114 (2019). [PubMed: 30640571]
5. https://clinicaltrials.gov.
6. Stopa N, Krebs JE & Shechter D The PRMT5 arginine methyltransferase: many roles in development, cancer and beyond. Cell. Mol. Life Sci 72, 2041–2059 (2015). [PubMed: 25662273]
7. Shailesh H, Zakaria ZZ, Baiocchi R & Sif S Protein arginine methyltransferase 5 (PRMT5) dysregulation in cancer. Oncotarget 9, 36705–36718 (2018). [PubMed: 30613353]
8. Kryukov GV et al. MTAP deletion confers enhanced dependency on the PRMT5 arginine methyltransferase in cancer cells. Science 351, 1214–1218 (2016). [PubMed: 26912360]
9. Marjon K et al. MTAP Deletions in Cancer Create Vulnerability to Targeting of the MAT2A/PRMT5/RIOK1 Axis. Cell Rep 15, 574–587 (2016). [PubMed: 27068473]
10. Mavrakis KJ et al. Disordered methionine metabolism in MTAP/CDKN2A-deleted cancers leads to dependence on PRMT5. Science 351, 1208–1213 (2016). [PubMed: 26912361]
11. Beroukhim R et al. The landscape of somatic copy-number alteration across human cancers. Nature 463, 899–905 (2010). [PubMed: 20164920]
12. Branscombe TL et al. PRMT5 (Janus kinase-binding protein 1) catalyzes the formation of symmetric dimethylarginine residues in proteins. J. Biol. Chem 276, 32971–32976 (2001). [PubMed: 11413150]
13. Rho J et al. Prmt5, which forms distinct homo-oligomers, is a member of the protein-arginine methyltransferase family. J. Biol. Chem 276, 11393–11401 (2001). [PubMed: 11152681]
14. Friesen WJ et al. A novel WD repeat protein component of the methylosome binds Sm proteins. J. Biol. Chem 277, 8243–8247 (2002). [PubMed: 11756452]
15. Antonysamy S et al. Crystal structure of the human PRMT5:MEP50 complex. Proc. Natl. Acad. Sci. U.S.A 109, 17960–17965 (2012). [PubMed: 23071334]
16. Burgos ES et al. Histone H2A and H4 N-terminal tails are positioned by the MEP50 WD repeat protein for efficient methylation by the PRMT5 arginine methyltransferase. J. Biol. Chem 290, 9674–9689 (2015). [PubMed: 25713080]
17. Gilbert LA et al. CRISPR-mediated modular RNA-guided regulation of transcription in eukaryotes. Cell 154, 442–451 (2013). [PubMed: 23849981]
18. Gilbert LA et al. Genome-Scale CRISPR-Mediated Control of Gene Repression and Activation. Cell 159, 647–661 (2014). [PubMed: 25307932]
19. Thompson A et al. Tandem mass tags: a novel quantification strategy for comparative analysis of complex protein mixtures by MS/MS. Anal. Chem 75, 1895–1904 (2003). [PubMed: 12713048]
20. McAlister GC et al. MultiNotch MS3 enables accurate, sensitive, and multiplexed detection of differential expression across cancer cell line proteomes. Anal. Chem. 86, 7150–7158 (2014). [PubMed: 24927332]

21. Wang T et al. Gene Essentiality Profiling Reveals Gene Networks and Synthetic Lethal Interactions with Oncogenic Ras. Cell 168, 890–903.e15 (2017). [PubMed: 28162770]
22. Braun CJ et al. Coordinated Splicing of Regulatory Detained Introns within Oncogenic Transcripts Creates an Exploitable Vulnerability in Malignant Glioma. Cancer Cell 32, 411–426.e11 (2017). [PubMed: 28966034]
23. Hamard P-J et al. PRMT5 Regulates DNA Repair by Controlling the Alternative Splicing of Histone-Modifying Enzymes. Cell Rep 24, 2643–2657 (2018). [PubMed: 30184499]
24. Rengasamy M et al. The PRMT5/WDR77 complex regulates alternative splicing through ZNF326 in breast cancer. Nucleic Acids Res. 1–15 (2017). doi:10.1093/nar/gkx727 [PubMed: 27899559]
25. Koh CM et al. MYC regulates the core pre-mRNA splicing machinery as an essential step in lymphomagenesis. Nature 523, 96–100 (2015). [PubMed: 25970242]
26. Bezzi M et al. Regulation of constitutive and alternative splicing by PRMT5 reveals a role for Mdm4 pre-mRNA in sensing defects in the spliceosomal machinery. Genes & Development 27, 1903–1916 (2013). [PubMed: 24013503]
27. Love MI, Huber W & Anders S Moderated estimation of fold change and dispersion for RNA-seq data with DESeq2. Genome Biology 15, 550 (2014). [PubMed: 25516281]
28. Robinson MD, McCarthy DJ & Smyth GK edgeR: a Bioconductor package for differential expression analysis of digital gene expression data. Bioinformatics 26, 139–140 (2010). [PubMed: 19910308]
29. Ritchie ME et al. limma powers differential expression analyses for RNA-sequencing and microarray studies. Nucleic Acids Res. 43, e47–e47 (2015). [PubMed: 25605792]
30. Trapnell C et al. Transcript assembly and quantification by RNA-Seq reveals unannotated transcripts and isoform switching during cell differentiation. Nat Biotechnol 28, 511–515 (2010). [PubMed: 20436464]
31. Anders S, Reyes A & Huber W Detecting differential usage of exons from RNA-seq data. Genome Research 22, 2008–2017 (2012). [PubMed: 22722343]
32. Hartley SW & Mullikin JC Detection and Visualization of Differential Splicing in RNA-Seq Data with JunctionSeq. arXiv.org q-bio.GN, e127 (2015).
33. Chandler SD, Mayeda A, Yeakley JM, Krainer AR & Fu XD RNA splicing specificity determined by the coordinated action of RNA recognition motifs in SR proteins. Proc Natl Acad Sci USA 94, 3596–3601 (1997). [PubMed: 9108022]
34. Hall-Pogar T, Liang S, Hague LK & Lutz CS Specific trans-acting proteins interact with auxiliary RNA polyadenylation elements in the COX-2 3'-UTR. RNA 13, 1103–1115 (2007). [PubMed: 17507659]
35. Melton AA, Jackson J, Wang J & Lynch KW Combinatorial control of signal-induced exon repression by hnRNP L and PSF. Mol. Cell. Biol 27, 6972–6984 (2007). [PubMed: 17664280]
36. Wang T et al. Gene Essentiality Profiling Reveals Gene Networks and Synthetic Lethal Interactions with Oncogenic Ras. Cell 168, 890–903.e15 (2017). [PubMed: 28162770]
37. Sinha R et al. Arginine methylation controls the subcellular localization and functions of the oncoprotein splicing factor SF2/ASF. Mol. Cell. Biol 30, 2762–2774 (2010). [PubMed: 20308322]
38. Das S & Krainer AR Emerging functions of SRSF1, splicing factor and oncoprotein, in RNA metabolism and cancer. Mol. Cancer Res. 12, 1195–1204 (2014). [PubMed: 24807918]
39. Twyffels L, Gueydan C & Kruys V Shuttling SR proteins: more than splicing factors. FEBS J. 278, 3246–3255 (2011). [PubMed: 21794093]
40. Zhang Z & Krainer AR Involvement of SR proteins in mRNA surveillance. MOLCEL 16, 597–607 (2004).
41. Kaushik S et al. Genetic deletion or small-molecule inhibition of the arginine methyltransferase PRMT5 exhibit anti-tumoral activity in mouse models of MLL-rearranged AML. Leukemia 32, 499–509 (2018). [PubMed: 28663579]
42. Musiani D et al. Proteomics profiling of arginine methylation defines PRMT5 substrate specificity. Sci Signal 12, eaat8388 (2019). [PubMed: 30940768]
43. Christoforou AL & Lilley KS Isobaric tagging approaches in quantitative proteomics: the ups and downs. Anal Bioanal Chem 404, 1029–1037 (2012). [PubMed: 22580419]

44. Cáceres JF, Screaton GR & Krainer AR A specific subset of SR proteins shuttles continuously between the nucleus and the cytoplasm. Genes & Development 12, 55–66 (1998). [PubMed: 9420331]

45. Krainer AR, Conway GC & Kozak D Purification and characterization of pre-mRNA splicing factor SF2 from HeLa cells. Genes & Development 4, 1158–1171 (1990). [PubMed: 2145194]

46. Krainer AR, Conway GC & Kozak D The essential pre-mRNA splicing factor SF2 influences 5' splice site selection by activating proximal sites. Cell 62, 35–42 (1990). [PubMed: 2364434]

47. Ge H & Manley JL A protein factor, ASF, controls cell-specific alternative splicing of SV40 early pre-mRNA in vitro. Cell 62, 25–34 (1990). [PubMed: 2163768]

48. da Silva MR et al. Splicing Regulators and Their Roles in Cancer Biology and Therapy. Biomed Res Int 2015, 150514–12 (2015). [PubMed: 26273588]

49. Xiang S et al. Phosphorylation drives a dynamic switch in serine/arginine-rich proteins. Structure 21, 2162–2174 (2013). [PubMed: 24183573]

50. Aubol BE et al. Processive phosphorylation of alternative splicing factor/splicing factor 2. Proc Natl Acad Sci USA 100, 12601–12606 (2003). [PubMed: 14555757]

51. Boutz PL, Bhutkar A & Sharp PA Detained introns are a novel, widespread class of post-transcriptionally spliced introns. Genes & Development 29, 63–80 (2015). [PubMed: 25561496]

52. Jacob AG & Smith CWJ Intron retention as a component of regulated gene expression programs. Hum. Genet 136, 1043–1057 (2017). [PubMed: 28391524]

53. Weatheritt RJ, Sterne-Weiler T & Blencowe BJ The ribosome-engaged landscape of alternative splicing. Nat. Struct. Mol. Biol 23, 1117–1123 (2016). [PubMed: 27820807]

Methods-only references

54. Radzisheuskaya A, Shlyueva D, Müller I & Helin K Optimizing sgRNA position markedly improves the efficiency of CRISPR/dCas9-mediated transcriptional repression. Nucleic Acids Res. 44, e141–e141 (2016). [PubMed: 27353328]

55. Ritchie ME et al. limma powers differential expression analyses for RNA-sequencing and microarray studies. Nucleic Acids Res. 43, e47 (2015). [PubMed: 25605792]

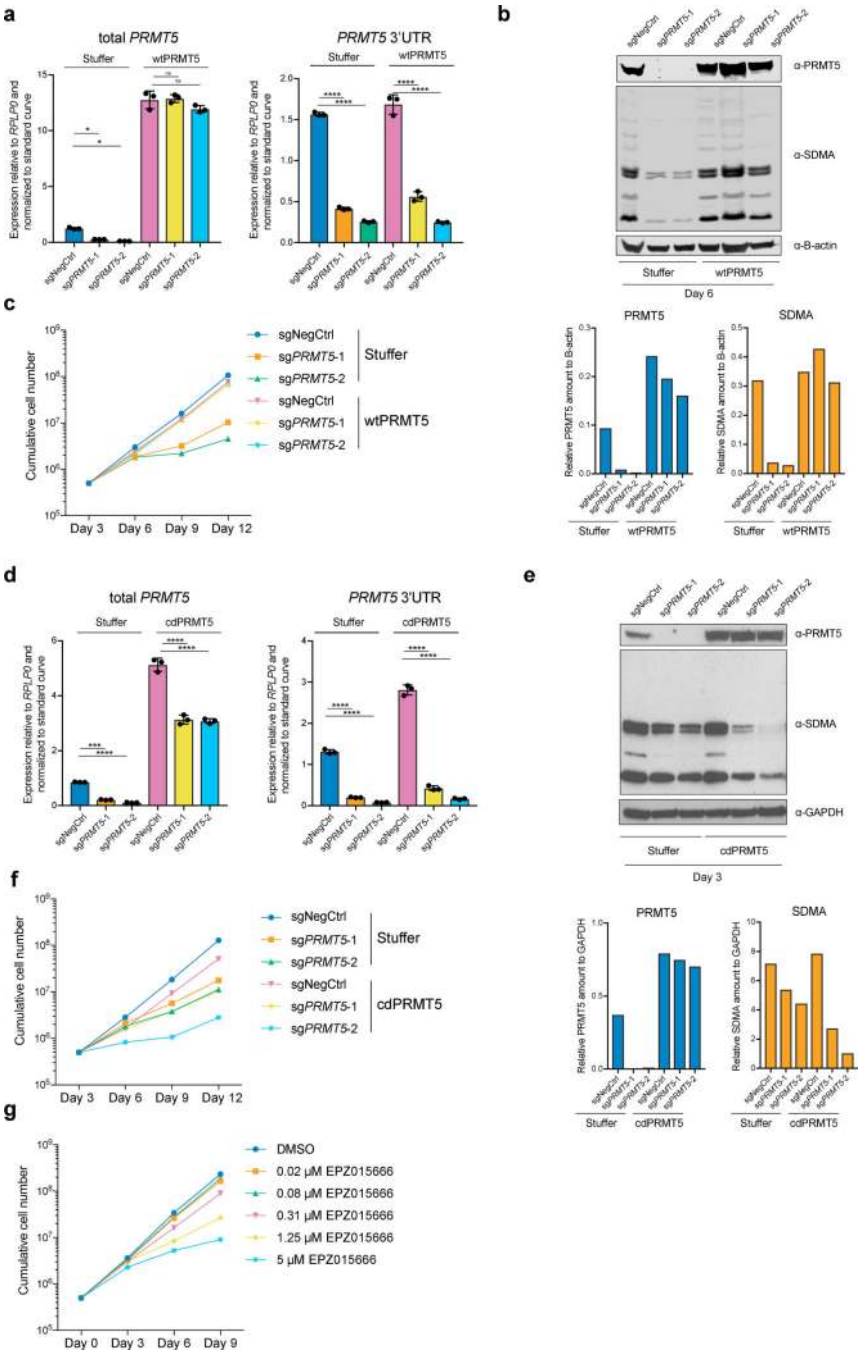

Figure 1. The catalytic activity of PRMT5 is required for proliferation of mouse and human MLL-AF9-rearranged AML cells.

a, qRT-PCR analysis of total and endogenous *PRMT5* expression in THP-1-cdCas9-KRAB-stuffer or wtPRMT5 cells transduced with either a non-targeting (NegCtrl) sgRNA or two sgRNAs against *PRMT5*. The values are normalized to *RPLP0* and shown as mean ±SD (n=3 technical replicates, * is $p < 0.05$, **** is $p < 0.0001$, "ns" is not significant according to Sidak's multiple comparisons test). **b,** Western blot analysis of PRMT5 and B-actin expression and symmetrical arginine dimethylation (SDMA) levels in THP-1-cdCas9-

KRAB-stuffer or wtPRMT5 cells transduced with either a non-targeting (NegCtrl) sgRNA or two sgRNAs against *PRMT5* six days after transduction. Bar chart shows quantification of protein levels relative to a loading control. **c,** Growth curves of THP-1-cdCas9-KRAB-stuffer or wtPRMT5 cells transduced with either a non-targeting (NegCtrl) sgRNA or two sgRNAs against *PRMT5*. X-axis indicates number of days after transduction. **d,** qRT-PCR analysis of total and endogenous *PRMT5* expression in THP-1-cdCas9-KRAB-stuffer or cdPRMT5 cells transduced with either a non-targeting (NegCtrl) sgRNA or two sgRNAs against *PRMT5*. The values are normalized to *RPLP0* and shown as mean ±SD (n=3 technical replicates, *** is $p < 0.001$, **** is $p < 0.0001$ according to Sidak's multiple comparisons test). **e,** Western blot analysis of PRMT5 and GAPDH expression and symmetrical arginine dimethylation (SDMA) levels in THP-1-cdCas9-KRAB-stuffer or cdPRMT5 cells transduced with either a non-targeting (NegCtrl) sgRNA or two sgRNAs against *PRMT5* three days after transduction. Bar chart shows quantification of protein levels relative to a loading control. **f,** Growth curves of THP-1-cdCas9-KRAB-stuffer or cdPRMT5 cells transduced with either a non-targeting (NegCtrl) sgRNA or two sgRNAs against *PRMT5*. X-axis indicates number of days after transduction. **g,** Growth curves of THP-1 cultured in DMSO or with the PRMT5 inhibitor EPZ015666 at different concentrations. X-axis indicates number of days after addition of the compound. The experiments in **a-c, g** were repeated three times independently with similar results. The experiments in **d-f** were repeated twice with similar results. Source data for **a-g** are available online. The uncropped westerns blots for **b** and **e** are shown in the Source Data.

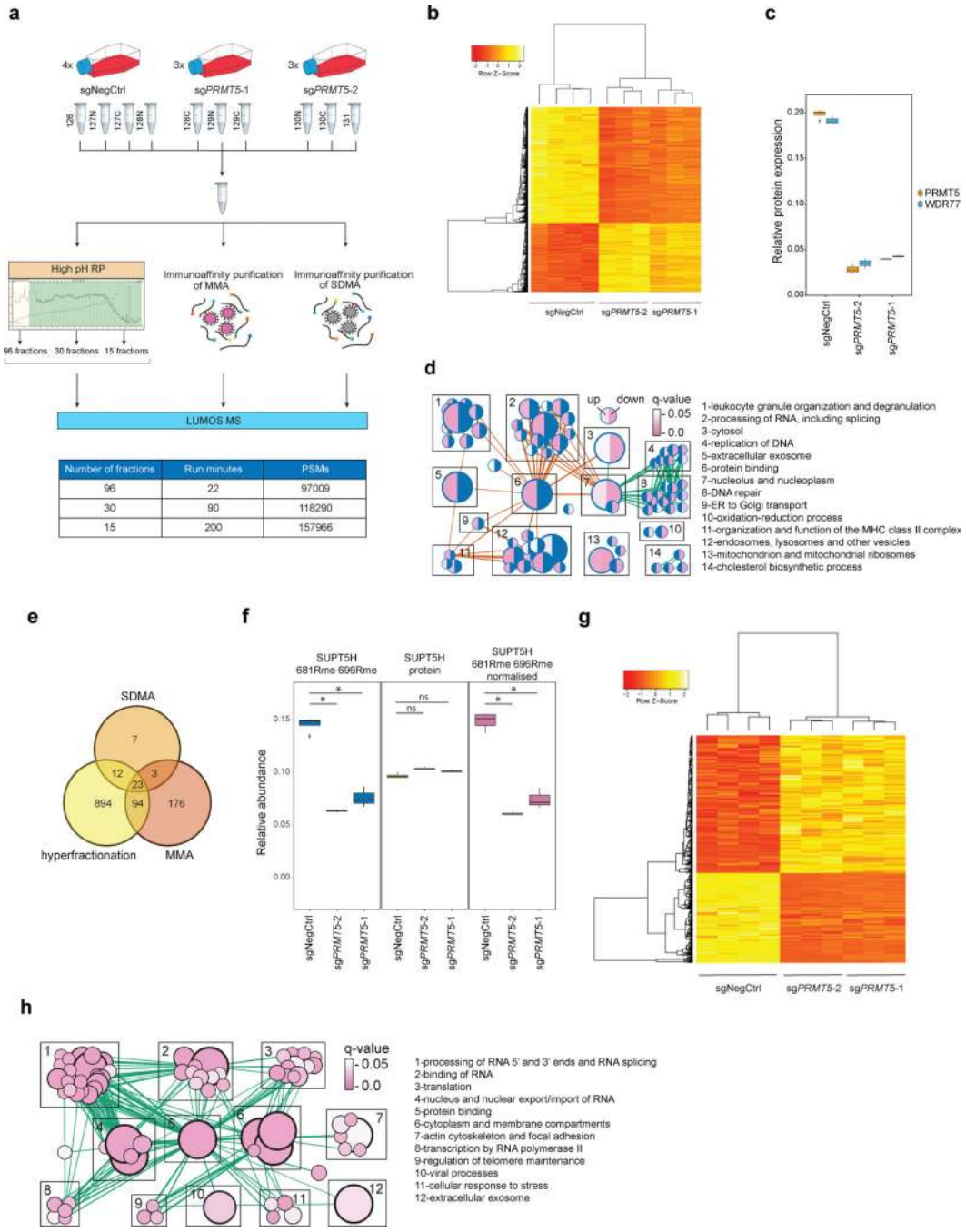

Figure 2. Proteome and methylome profiling identify novel PRMT5 substrates in human AML cells.

a, Outline of the proteome and methylome profiling strategies in THP-1-cdCas9-KRAB cells transduced with a non-targeting sgRNA (NegCtrl) or two independent sgRNAs against *PRMT5* (see methods for details). MMA = monomethylated arginine, SDMA = symmetrically dimethylated arginine, high pH RP = high pH reverse phase chromatography, PSMs = peptide spectrum matches. **b,** Heatmap of 2962 differentially expressed proteins (q-value ≤0.05 in both sgRNAs, limma test, with p-values adjusted by Storey method). **c,**

Boxplot representing relative protein abundance of PRMT5 and its co-factor WDR77 in THP-1-cdCas9-KRAB cells transduced with non-targeting sgRNA (NegCtrl) or two independent sgRNAs against *PRMT5*. Boxplot summary: outliers (points), minimum (lower whisker), first quartile (lower bound of box), median (horizontal line inside box), third quartile (upper bound of box), interquartile range (box), and maximum (upper whisker). For PRMT5-depleted cells, n=3 independently transduced samples. For wild-type cells, n=4 independently transduced samples. The difference between the negative control and each of the knockdown sgRNA is statistically significant (q-value < 0.05, limma test, with p-values adjusted by Storey method). **d,** Gene Ontology-based functional classification of 2962 up- and downregulated proteins in THP-1 cells following *PRMT5* knockdown (two-sided Fisher's exact test, FDR-adjusted p-value < 0.05). The nodes represent significantly enriched protein sets, node size is proportional to the number of members in a protein set, and color intensity reflects the q-value. Edges indicate the protein overlap between the nodes with thicker edges indicating higher degree of overlap. Orange edges illustrate upregulated categories, green – downregulated. Functionally related protein sets are clustered, numbered and named. Blue color in half circles indicates no enriched categories. **e,** Venn diagram representing the number of methylated peptides identified using the strategies outlined in Fig.2a. **f,** An example of normalization of the arginine methylation site quantified against the protein level. 681R and 696R methylation sites of SUPT5H were quantified as decreasing upon *PRMT5* knockdown, while the SUPT5H protein itself was, conversely, slightly upregulated. Hence, normalization results in the increased fold change for methylation site quantification. Rme = arginine methylation. Boxplot summary as in c. For PRMT5-depleted cells, n=3 independently transduced samples. For wild-type cells, n=4 independently transduced samples. **g,** Heatmap of 420 differentially methylated sites. (q-value ≤0.1 in both sgRNAs, limma test, with p-values adjusted by Storey method). **h,** Enrichment map of the Gene Ontology-enriched protein sets across 61 identified potential PRMT5 targets. Representation and statistics as in panel d. The proteomics experiments were performed using three independently transduced samples of PRMT5-depleted cells (two independent sgRNAs) and four independently transduced samples of wild-type cells. Source data are available in Supplementary Table 1.

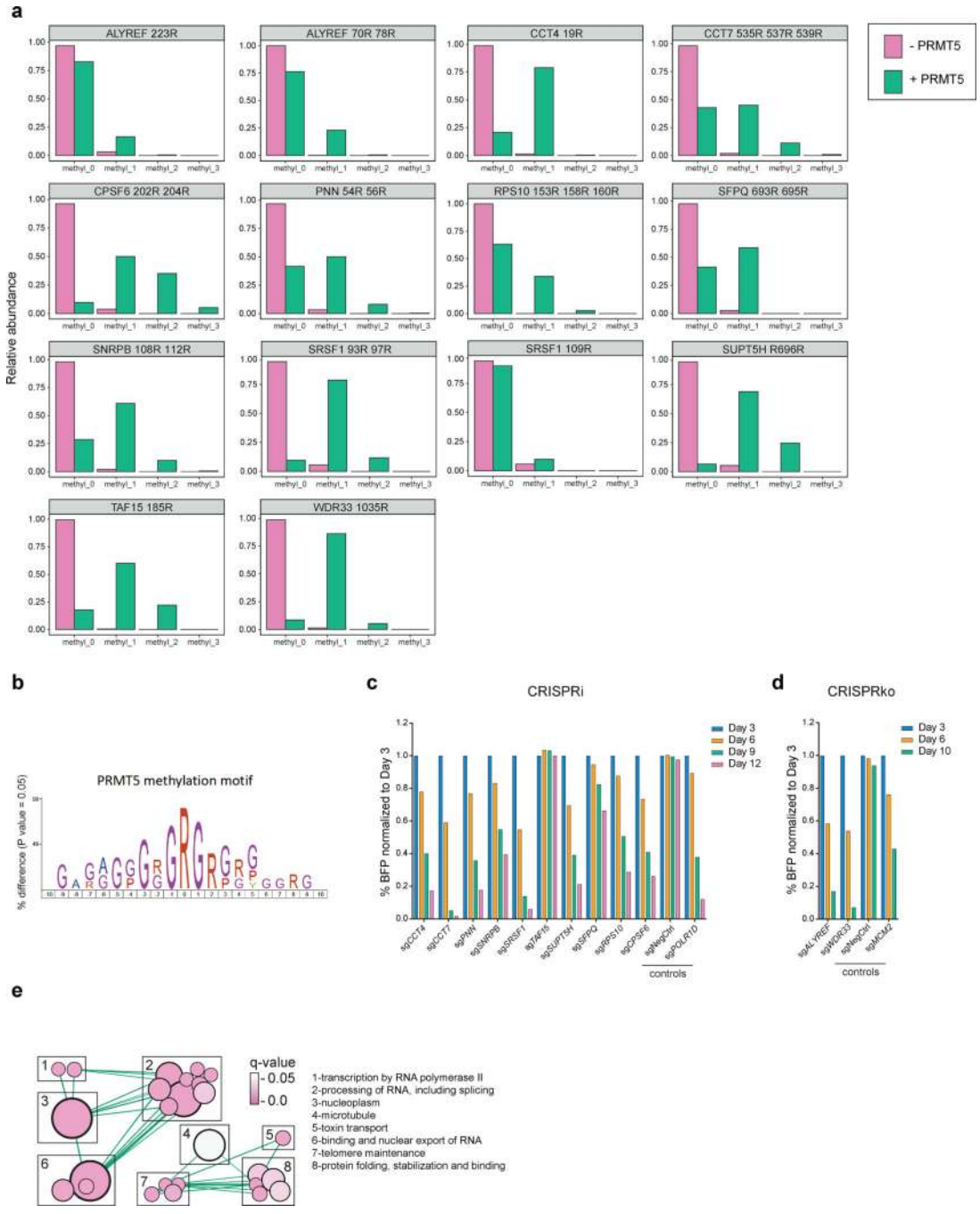

Figure 3. Validation of the essential PRMT5 substrates.

a, Distributions of abundances of unmethylated and methylated peptide forms after the incubation with or without recombinant PRMT5-WDR77 complex. Only the peptides belonging to the confirmed PRMT5 substrates are shown here. **b,** PRMT5 methylation motif predicted using an iceLogo tool. Y axis represents the difference between the frequency of an amino acid in a sample set and the reference set (human proteome). **c,** CRISPRi competition assays to confirm essentiality of *CCT4*, *CCT7*, *PNN*, *SNRPB*, *SRSF1*, *TAF15*, *SUPT5H*, *SFPQ*, *RPS10* and *CPSF6*. THP-1-cdCas9-KRAB cells were transduced with the

sgRNAs against the genes of interest and the percentage of sgRNA-transduced (BFP-positive) cells was measured over time. An sgRNA targeting *POLR1D* was used as a positive control and a non-targeting sgRNA (NegCtrl) was used as a negative control. **d,** CRISPRko competition assays to confirm essentiality of *ALYREF* and *WDR33*. THP-1-wtCas9 cells were transduced with lentiviruses expressing the sgRNAs against the genes of interest and the percentage of sgRNA-transduced (BFP-positive) cells was measured over time. An sgRNA targeting *MCM2* was used as a positive control and a non-targeting sgRNA (NegCtrl) was used as a negative control. **e,** Enrichment map of the Gene Ontology-enriched protein sets across 11 validated essential substrates of PRMT5 (two-sided Fisher's exact test, FDR-adjusted p-value < 0.05). Nodes represent significantly enriched protein sets, node size is proportional to the number of members in a protein set, and color intensity depends on the q-value. Edges indicate the protein overlap between the nodes with thicker edges indicating higher overlap between the nodes. Functionally related protein sets are clustered, numbered and named. The experiments in **a, c, d** were repeated twice with similar results. Source data for **a** are available in Supplementary Table 1. Source data for **c,d** are available online.

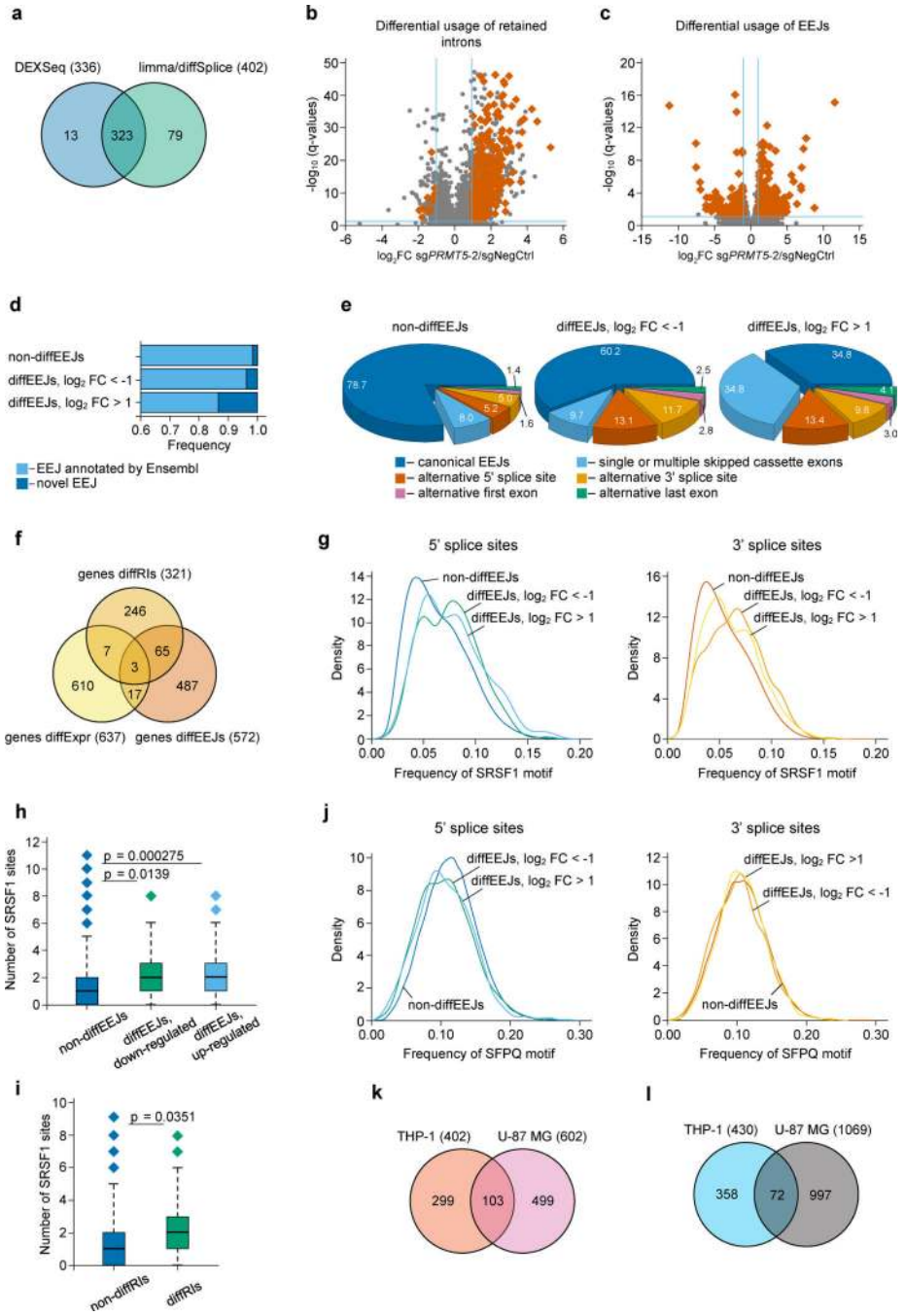

Figure 4. PRMT5 depletion leads to changes in alternative splicing in human AML cells.

a, DEXSeq and limma-diffSplice algorithms show the differential usage of 415 RIs in the transcriptome of THP-1 cells following *PRMT5* knockdown (more than 2-fold changes, p-value < 0.002, q-value < 0.05). **b,** Volcano plot demonstrating the differential usage of retained introns in the transcriptome of THP-1 cells upon *PRMT5* knockdown (total 109530 events). RIs were included in differential analysis as expressed exons, and 336 diffRIs are shown using dark orange squares. The vertical dashed lines represent two-fold differences between the *PRMT5* knockdown and wild type cells and horizontal dashed line shows the

FDR adjusted q-value threshold of 0.05. These results were generated using DEXSeq algorithm, and very similar results were observed with limma-diffSplice approach. **c,** Volcano plot demonstrating the differential usage of EEJs in the transcriptome of THP-1 cells upon *PRMT5* knockdown (total 76434 exon-exon junctions). 430 DiffEEJs are shown by dark orange squares. The vertical dashed lines represent two-fold differences between the *PRMT5* knockdown and wild type cells, and horizontal dashed line shows the FDR adjusted q-value threshold of 0.05. These results were generated using limma-diffSplice algorithm. **d,** The majority of the identified non-diffEEJs or diffEEJs are annotated in the Ensembl database (GRCh38.p7 assembly of human genome, release 85, July 2016), and only small fractions of EEJs are new junctions. The following numbers of EEJs were analyzed: non-diffEEJs – 76004, diffEEJs $\log_2$FC < −1 – 184, diffEEJs $\log_2$FC > 1 – 246). **e,** Classification of non-diffEEJs and diffEEJs according to main modes, or types, of alternative splicing. The identified EEJs were divided in three sub-sets: i) non-diffEEJs, ii) diffEEJs with prevalence in the control cells (logFC < –1), and iii) diffEEJs with prevalence in the cells with *PRMT5* knockdown (logFC > 1). Classification was carried out using Ensembl-based models of hypothetical non-alternative preRNAs of human genes. Numbers show the percentage of EEJs assigned to a particular mode of alternative splicing. **f,** Venn diagram demonstrating minimal overlap between the lists of differentially expressed genes (genes diffExpr), genes with diffRIs (genes diffRIs) and genes with diffEEJs (genes diffEEJs). **g,** Density diagrams of SRSF1 motif frequency at the 5’ and 3’ splice sites of the differential and non-differential EEJs (dynamic thresholding). **h-i,** Median absolute numbers of SRSF1 motifs in differential and non-differential EEJs (**h**) and RIs (**i**) (fixed thresholding, two-sided Mann-Whitney U test). Boxplot summary (**h,i**): outliers (diamonds), minimum (lower whisker), first quartile (lower bound of box), median (horizontal line inside box), third quartile (upper bound of box), interquartile range (box), and maximum (upper whisker). The following numbers of splicing events were compared: non-diffEEJs – 76004, difEEJs downregulated – 184, diffEEJs upregulated – 246, non-diffRIs – 1540, diffRIs – 336. **j,** Density diagrams of SFPQ motif frequency at the 5’ and 3’ splice sites of the differential and non-differential EEJs (dynamic thresholding). **k-l,** Venn diagrams of the overlapping lists of the differentially used EEJs (**k**) and RIs (**l**) identified in THP-1 and U-87 MG cells upon *PRMT5* KD. The splicing analysis experiments were performed using three independently transduced samples of each sgRNA. Source data are available in Supplementary Table 2.

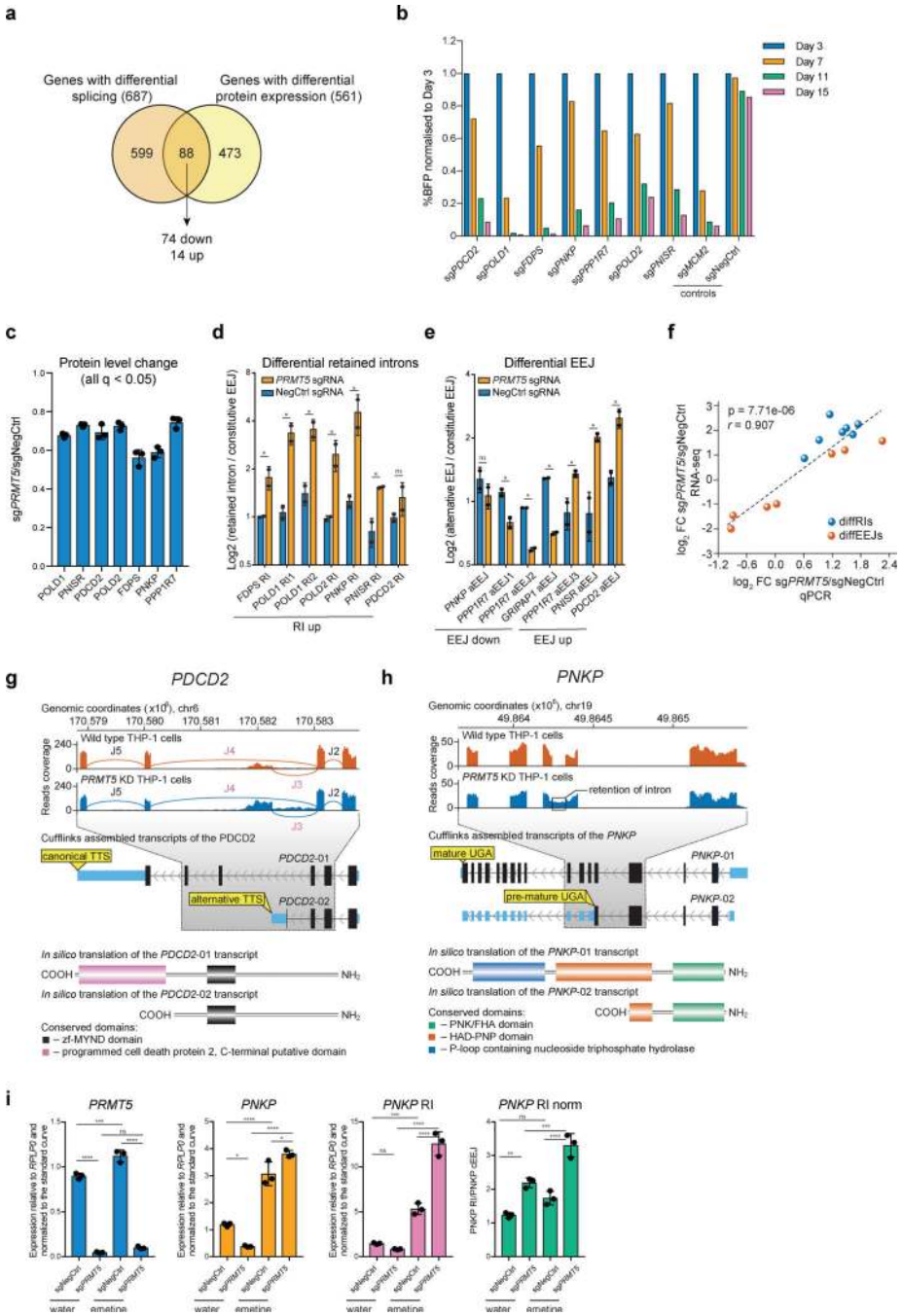

Figure 5. PRMT5 loss induces alternative splicing and reduction in protein level of multiple essential genes.

a, Venn diagram showing that among the 826 differentially spliced genes in the *PRMT5* KD cells, 88 also exhibited change in their total protein levels, of which 74 proteins were downregulated and 14 proteins upregulated. **b,** Competition assays of THP-1-wtCas9 cells transduced with the sgRNAs targeting the genes of interest. The percentage of sgRNA-transduced (BFP-positive) cells was measured over time. An sgRNA against *MCM2* was used as a positive control and a non-targeting sgRNA (NegCtrl) was used as a negative

control. **c,** Barplot representing changes in protein abundance of the selected candidates upon the knockdown of *PRMT5*. The values are mean±SD. For PRMT5-depleted cells, n=3 independently transduced samples. For wild-type cells, n=4 independently transduced samples. The values are shown relative to NegCtrl sgRNA (q-value < 0.05, limma test, with p-values adjusted by Storey method). **d,** qRT-PCR validation of the identified differential retained intron events. The values represent mean±SD of two independent transductions. * is p-value < 0.1, "ns" is not significant according to an unpaired t test. **e,** qRT-PCR validation of the identified differential EEJ. The values represent mean±SD of two independent transductions. The differential EEJ of the *GRIPAP1* gene was added as an example of an exon skipping event, which is a predominant mode of the upregulated alternative splicing events in the *PRMT5* KD cells. * is p-value < 0.1, "ns" is not significant according to an unpaired t test. **f,** Scatter plot demonstrating the correlation between the $\log_2$FC of the differential splicing events obtained using RNA-seq (n=3 independent transductions) and qPCR approaches (n=2 independent transductions) (two-sided Student t-test). **g-h,** Schematic representation of the differential alternative splicing events in *PDCD2* (g) and *PNKP* (h) RNA transcripts. In (g), EEJs are designated by the letter J and numbered. The concomitant statistics for these junctions are as follows: J2 (log2 FC = 0.22, q = 0.846), J3 (log2 FC = 1.23; q = 2.53E-02), J4 (log2 FC = −0.76; q = 0.034) and J5 (log2 FC = −0.31; q = 0.708). The differential splicing events are highlighted in purple. **i,** qRT-PCR analysis of the levels of *PRMT5*, constitutive *PNKP* EEJ (*PNKP* cEEJ) and *PNKP* retained intron (*PNKP* RI) in the cells transduced either with a negative control or a sgRNA targeting *PRMT5* and treated with emetine or water for 3 hours. "*PNKP* RI norm" stands for the expression of the *PNKP* RI normalized to the levels of *PNKP* cEEJ. The values are mean ± SD (n=3 technical replicates, * is p-value < 0.01, ** is p-value < 0.005, *** is p-value < 0.001, **** is p-value < 0.0001, "ns" is not significant according to Sidak's multiple comparisons test). The experiment in **b** was repeated three times independently with similar results. The experiments in **d, e** were performed in two independent viral transductions. The experiment in **i** was performed in three independent viral transductions, which where pooled prior to qRT-PCR analysis. Source data for **b, d-f, i** are available online. Source data for **c, f** are available in Supplementary Table 1 and 2, respectively.

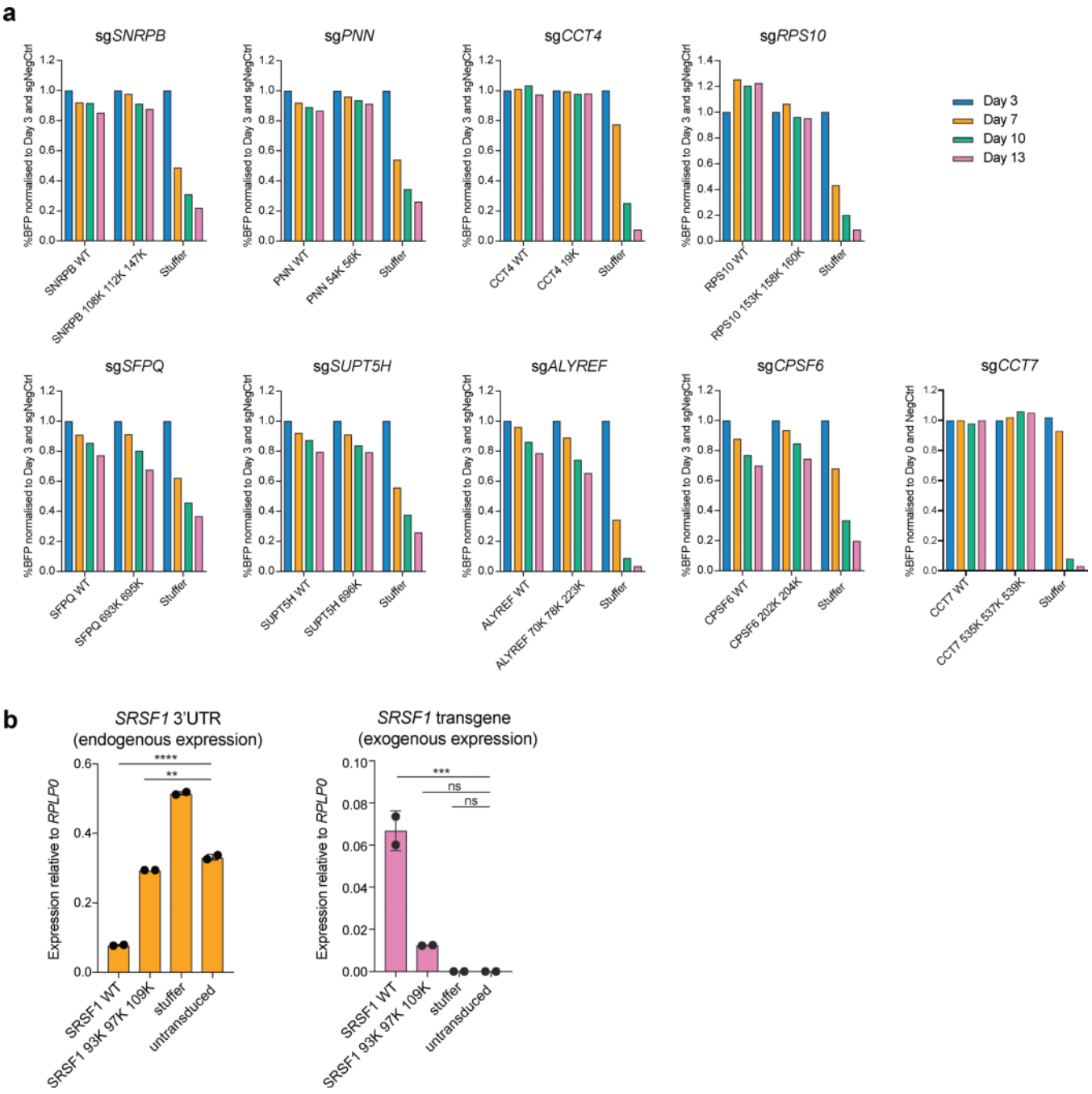

Figure 6. Arginine methylation of SRSF1 is functionally important for cell survival.

a, Competition assays to assess the functionality of the R-to-K mutants of the essential PRMT5 substrates. Cell lines stably expressing either the wild type or mutant versions of each substrate were transduced with an sgRNA against the substrate of interest. After the transduction, the percentage of BFP positive (sgRNA-expressing) cells was monitored over time. **b,** qRT-PCR analysis of the endogenous (3'UTR) and exogenous *SRSF1* expression in BFP and mCherry double positive cells co-transduced with an sgRNA targeting *SRSF1* and either SRSF1 WT or mutant cDNA or a stuffer construct. The values are normalized to

RPLP0 and shown as mean ±SD (n=2 technical replicates, ** is p-value < 0.01, *** is p-value < 0.001, **** is p-value < 0.0001, “ns” is non-significant according to Sidak’s multiple comparisons test). The experiments in **a** and **b** were repeated twice with similar results. The source data are available online.

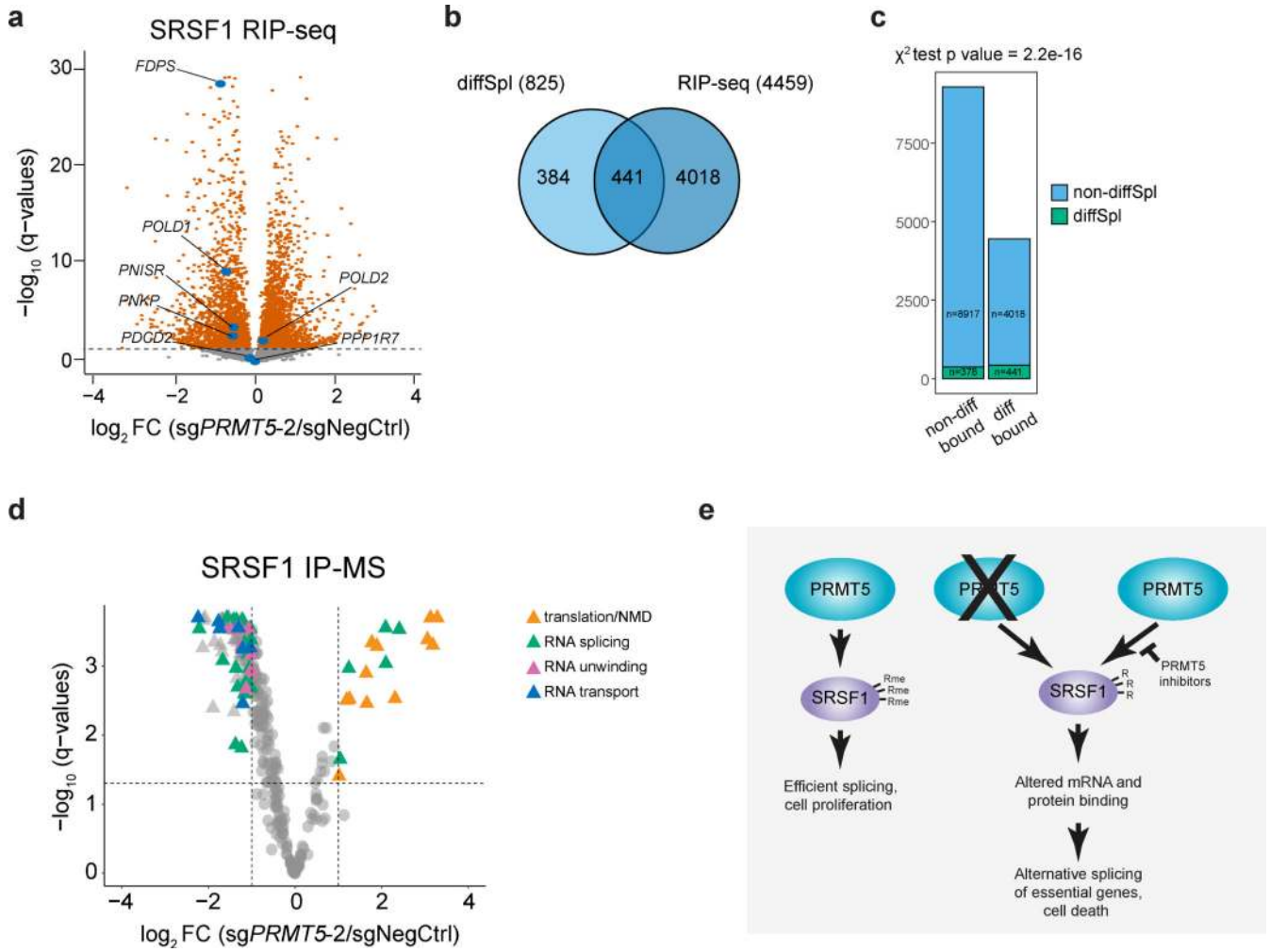

Figure 7. PRMT5 depletion impacts SRSF1 binding to mRNAs and proteins.

a, Differential binding of SRSF1 to mRNAs upon *PRMT5* KD (differentially bound mRNAs are represented by orange color, q-value < 0.05). mRNAs of 13754 genes were identified of which 4459 were differentially bound. **b,** Overlap of differentially spliced genes with the genes, which mRNAs are differentially bound by SRSF1 upon *PRMT5* KD. **c,** Distribution of differentially spliced genes among the genes with differentially or non-differentially bound mRNAs. **d,** Differential binding of SRSF1 to proteins upon *PRMT5* KD. Dashed lines indicate the chosen thresholds of 2-fold change and q-value of 0.05. Total of 350 binding partners were quantified, and 162 significantly differentially bound proteins are indicated with triangles. The most enriched functional groups of proteins among the differential interactors are indicated with color. **e,** Proposed model for the essential function of PRMT5. PRMT5 methylates SRSF1 at three arginine sites, which are important for the function of SRSF1 in splicing regulation. Loss of SRSF1 methylation leads to altered binding of SRSF1 to mRNA and proteins, differential alternative splicing of multiple essential genes and, consequently, cell death. RIP-sequencing and SRSF1 IP-MS

experiments were performed using 3 independently transduced samples of each sgRNA. The source data for the figure is available in Supplementary Tables 3 and 4.

Table 1.

A list of the validated essential PRMT5 substrates.

Substrate name	Description
ALYREF	Aly/REF Export Factor
SUPT5H	Transcription elongation factor
CPSF6	Cleavage and Polyadenylation Specific Factor 6
SNRPB	Small Nuclear Ribonucleoprotein Polypeptides B and B1
SFPQ	Splicing Factor Proline and Glutamine Rich
PNN	Pinin
SRSF1	Serine and Arginine Rich Splicing Factor 1
WDR33	pre-mRNA 3'end processing protein
RPS10	Ribosomal Protein S10
CCT4	T-complex protein 1 subunit delta
CCT7	T-complex protein 1 subunit eta

*in green – published PRMT5 substrates

Table 2.

Summary of the top gene ontology categories for the decreased SRSF1 interactors.

Top categories for decreased interactors		
Term	**Fold enrichment**	**Adjusted p-value**
GO:0000398~mRNA splicing	17.19	1.04E-24
GO:0010501~mRNA unwinding	26.02	2.65E-07
GO:0051028~mRNA transport	21.65	8.29E-06

Table 3.

Summary of the top gene ontology categories for the increased SRSF1 interactors.

Top categories for increased interactors		
Term	**Fold enrichment**	**Adjusted p-value**
GO:0006412~translation	41.92	3.00E-15
GO:0000398~mRNA splicing	23.89	3.29E-05